

POLITECNICO DI TORINO

Thesis for Master of Science degree in Aerospace Engineering

Development and Analysis of a Two-Stage-To-Orbit Orbit Re-entry Corridor Requirements



Tutor

prof. Nicole Viola

Co-Tutor

prof. Davide Ferretto

prof. Roberta Fusaro

prof. Oscar Gori

Author

Andrea Civita

June 2022

Abstract

Since the first Wright Brothers flight, there has been a continuous development of new kinds of vehicles to make aviation safer, faster, and cheaper. The last of these innovative projects is STRATOFLY, financed by the European Commission, a new type of civil aircraft for high-speed flight over antipodal routes. STRATOFLY, in the next future, is going to carry passengers from Bruxelles to Sydney in just a few hours. It will be possible thanks to the high cruise altitude in the stratosphere and to the Mach 8 speed reached.

From this kind of concept, it is possible to evolve new varieties of vehicles, towards Two-Stages To Orbit (TSTO) with many different mission profiles.

This Thesis aims at building high-level requirements for a second stage atmosphere re-entry, studying the re-entry corridor, the correlation with take-off requirements, and determining the best trade-off between landing and take-off requirements.

The study starts with a statistical analysis of similar vehicle performances. The following step is building the re-entry corridor for a given aircraft and payload weight, obtaining attitude parameters for the descending slope.

If landing parameters conflict with take-off ones, an optimizing cycle solves the critical issues.

In the end, all the parameters are collected in a matching chart which provides information on the design point.

Contents

Abstract.....	1
Chapter 1.....	1
Introduction.....	1
STRATOFLY.....	1
1.1 Partnership & Objectives.....	1
1.2 STRATOFLY MR3 Design.....	3
1.3 Propulsive Subsystem.....	5
1.4 Aerodynamics.....	11
1.5 Thermal Protection Subsystem.....	14
1.6 Thermal and Energy Management Subsystem.....	15
Chapter 2.....	17
Statistical analysis.....	17
1.1 Space Shuttle [14].....	17
2.2 X-33 [14] [15].....	22
3.3 X-34 [14] [15].....	24
4.2 Hope-X [14].....	27
5.2 Hermes [14] [16].....	30
6.2 Sanger and Horus [14] [17].....	36
6.3 Conclusions.....	41
Chapter 3.....	44
Atmospheric Re-Entry.....	44
3.1 Introduction.....	44
3.2 Entry Corridor.....	45
3.3 Constraint Boundaries.....	46
Chapter 4.....	49
Matlab Model.....	49
4.1 Objectives.....	49
4.2 Boundary Equation.....	50
4.3 Performance Invariant Quantities.....	54

4.4 Optimization cycle for re-entry corridor requirements.....	55
4.5 Matching Chart.....	56
4.6 Numerical Evaluation	61
4.7 Comparison with Sanger.....	64
4.8 Conclusions and future studies.....	66
Bibliography	67

Chapter 1

Introduction

The purpose of this work is to define high-level performance requirements for an atmosphere re-entry and a matching chart for a new concept of Two-Stage To Orbit. This new vehicle is going to be able to carry human and non-human payloads in low Earth orbit.

The starting point of this study is a statistical analysis of previous orbital vehicles, in order to define average curves for lift, drag, and aerodynamic efficiency. Regarding the first stage, the chosen model is STRATOFLY MR3, as well for all the systems and sub-systems. So all the parameters are related to this European innovative concept.

This first chapter introduces and describes the STRATOFLY project, introducing its state of art, developments, aerodynamics, and main subsystems.

STRATOFLY

1.1 Partnership & Objectives

The *STRATOFLY* project (STRATOspheric FLYing Opportunities for High-Speed Propulsion Concepts) was launched by European Union's Horizon 2020 research and innovation program in June 2018 [1]. This big European allocation of funds aims at developing new technologies supporting an open search policy in every scientific field. [2]



Figure 1 Stratofly logo [2]

Specifically, Research and Innovation Action in the field of Smart, Green and Integrated Transport within the H2020 Call for ‘Mobility for Growth’, in the area of ‘Breakthrough Innovation in Aviation’ was carried out thanks to the collaboration of several European institutions spread in 7 different countries, led by Politecnico di Torino [3]:

- Politecnico di Torino, Italy. Project Coordinator.
- Centro Italiano Ricerche Aerospaziali (CIRA), Italy
- Institut Von Karman De Dynamique Des Fluides, Belgium
- Stichting Nationaal Lucht- En Ruimtevaartlaboratorium, Holland
- Deutsches Zentrum Fuer Luft - Und Raumfahrt Ev, Germany
- Technische Universitat Hamburg-Harburg, Germany
- Fundacion de la Ingenieria Civil De Galicia, Spain
- Office National d'Etudes et de Recherches Aerospatiales, France
- Centre National de La Recherche Scientifique Cnrs, France
- Totalforsvarets Forskningsinstitut, Sweden.

STRATOFLY explores the open frontier of civil high-speed passenger stratospheric flight. Conventional planes fly in the lower layer of the atmosphere leaving the upper one to new exploitation for commercial purposes. In the next few years, the number of passengers will increase significantly, and the airline companies will have to be capable to open new routes up to meet the growing demand.

STRATOFLY operates in this scenario, refining the design of hypersonic vehicles at high altitudes (10,000km) and high speeds (Mach 8). It also aims at improving sustainability, cutting fuel consumption, CO₂ and NO_x emission per passenger, and noise. [4]

Summing up the main objectives of this project are:

- Optimization of the innovative hypersonic vehicle concept to operate civil passenger transportation in the upper atmosphere;
- Increase embedded high-speed propulsion systems performances;
- Minimize environmental impact;
- Increase Technology Readiness Level (TRL) of enabling technologies up to 6 by 2035
- Decrease time in long-range flight
- Incorporate multi-functional systems
- Study stratospheric routes for civil flights
- Minimize environmental impact;
- Evaluate new technologies for future developments. [5]

1.2 STRATOFLY MR3 Design

STRATOFLY MR3 is shaped with a waderider configuration and bubble structure with engines located on top of the dorsal spine. Fuel is stored in a multi-lobe tank architecture which maximizes the capacity and minimizes the weight. Payload and passengers are located in the ventral part of the vehicle.



Figure 2 STRATOFLY Concept

STRATOFLY MR3 design has many parts in common with its predecessor, LAPCAT MR2.4, with some improvements. They have almost the same configuration with about 400 tons of Maximum Take-Off Weight (MTOW) and 94 m of length. To perform their mission, they can carry up to 300 passengers and operate with similar subsystems and performances in a stratospheric cruise at 30-35 km of altitude at Mach 8.



Figure 3 a) STRATOFLY MR3 vehicle concept - b) LAPCAT MR2.4 vehicle concept

There are several differences between the inner and outer layout concepts. First of all, the preliminary version of the STRATOFLY MR3 doesn't have canards on the nose, because they are not necessary anymore thanks to the new shape. Although the cabin volume is quite similar, 1200m² to 1400m², the passengers are located differently due to the new subsystems location, such as tanks and engines, and safety reasons like boarding procedure and escape routes. Furthermore, the cabin location has been adjusted to the CoG to have better performances during the mission, meeting weight & balance needs. [6] [7]

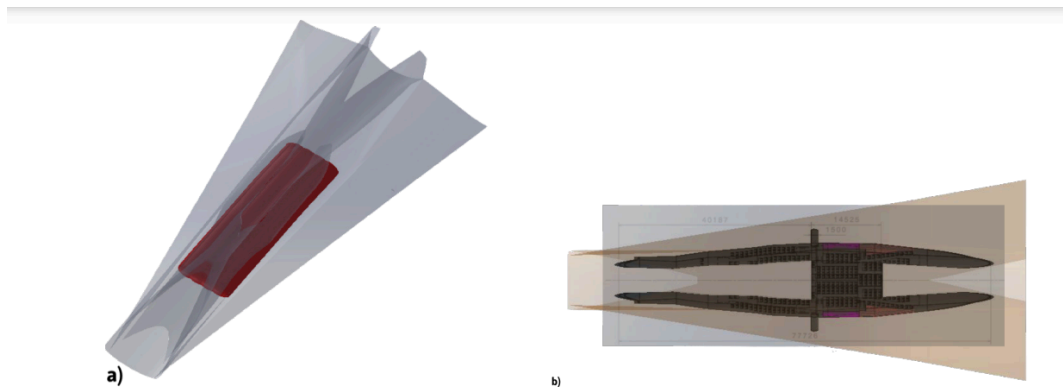


Figure 4a) STRATOFLY passenger cabin design - b) LAPCAT passenger cabin design

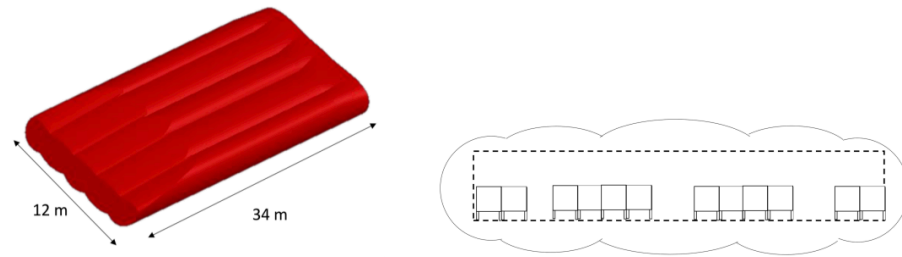


Figure 5 STRATOFLY passengers cabin dimensions and seats configuration

Systems and subsystems are still under development, and those for which a higher detail is available are listed hereafter:

- Thermal and Energy Management Subsystem (TEMS);
- Environmental Control and Life Support Subsystem (ECLSS);
- Thermal Protection Subsystem (TPS);
- Propulsive subsystem;

The following subsystems are just developed at a high level, engineering general characteristics, weight, and power budget:

- Landing Gear;
- Propellant Subsystem;
- Electric Subsystem;
- Avionic Subsystem;
- Flight Control System (FCS).

1.3 Propulsive Subsystem

LAPCAT propulsion subsystem is utilized by STRATOFLY too, so the performances studied in previous reports will stand. [8]

The propulsion subsystem is located on top of the vehicle and it's formed by two different kinds of engines that are activated depending on the flight condition defined by the mission: speed, altitude, and range. The engines are composed of two different units which work at different speeds.

Air Turbo Rocket (ATR) engine works from 0 Mach to 4-4.5 Mach and it's capable of take-off and landing. There are 6 of them housed in two different bays, one on each side of the fuselage. They use a mix of a turbojet Bryton

cycle and Rankine cycle of an expander rocket [9]. The intake is based on a previous XB-70 U.S. Air Force. model 2D air intake. At last, the exhaust gas passes through a convergent-divergent nozzle, increasing its speed, and finally into the central main nozzle to complete the expansion.

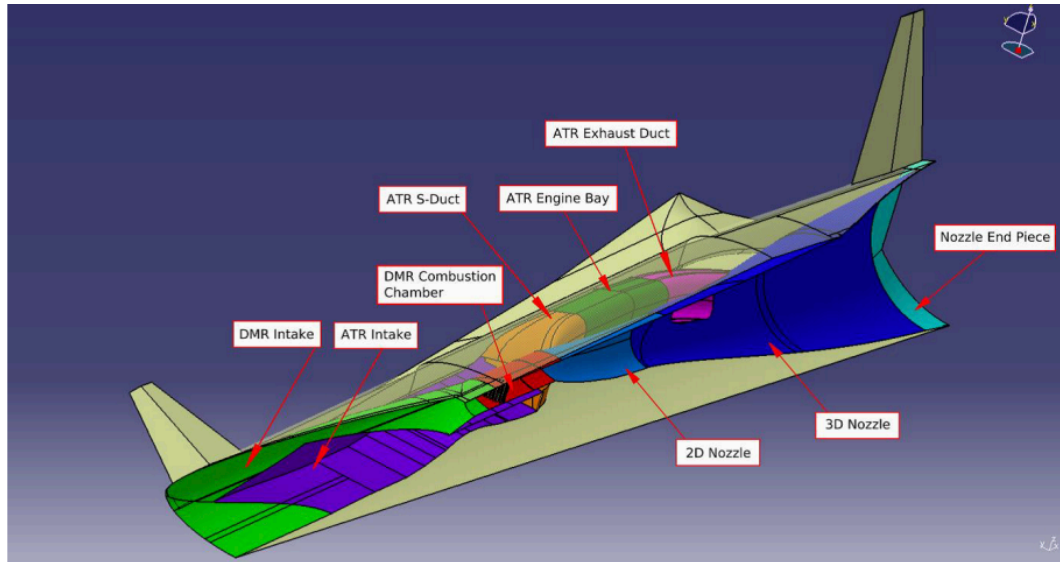


Figure 6 Propulsion Subsystem

Dual Mode Ramjet (DMR) works at hypersonic speed from 4.5 Mach to 8 Mach and is located in the center. First, the flow pass through an elliptical air intake, the ratio between major and minor axis is three, then into an elliptical combustion chamber with nearly constant section. The nozzle is composed of two sequential stages. A 2D nozzle merges elliptical flux into a circular 3D flux. Its ratio is three and it is 13m long. The following nozzle is the 3D one, a truncated isentropic expansion nozzle, with a ratio of ten and 40m long. At last, a cone is placed to match the nozzle with the external shape of the fuselage [10] [11].

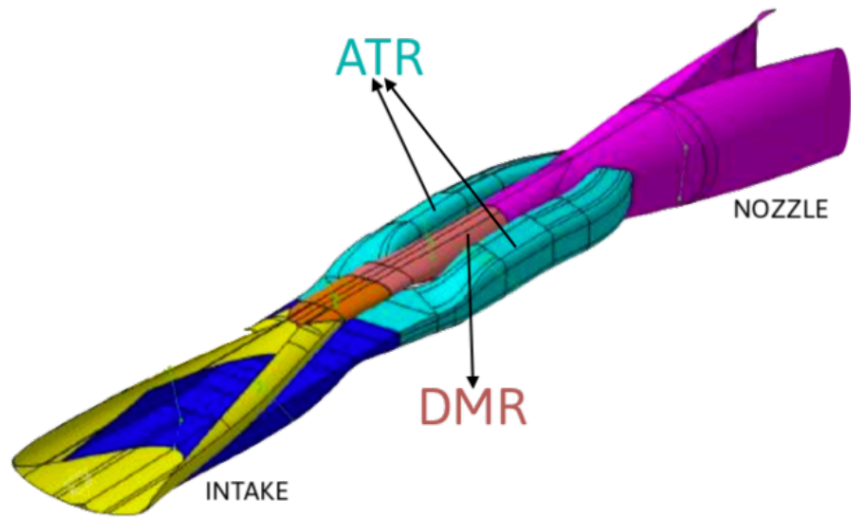


Figure 7 Illustration of the Propulsive Subsystem

In order to reduce waste of space and mass, the fuel required by the engines is the same and it is liquid hydrogen (LH2).

ATR and DMR mainly work separately, at low-speed DMR is shut down, although part of unburned flow passes through its combustion chamber, at high-speed ATR intake and nozzle are closed by sliding doors. But both cooperate in the speed range between 3 Mach and 4.5 Mach.

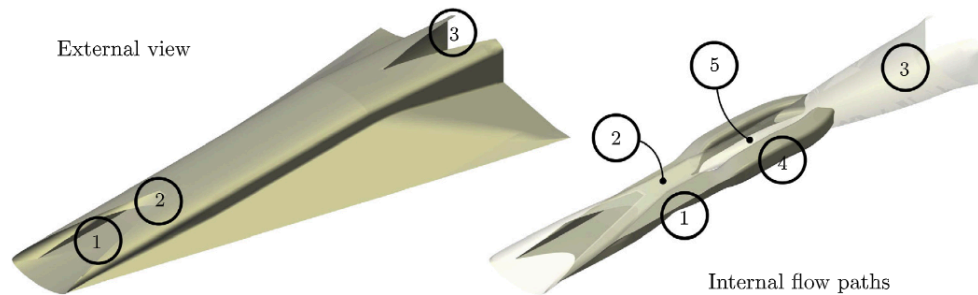


Figure 8 Rendering of the Mach 8 cruise aircraft: 1 low-speed intake, 2 high-speed intake, 3 nozzle, 4 ATR duct, 5 DMR duct [9]

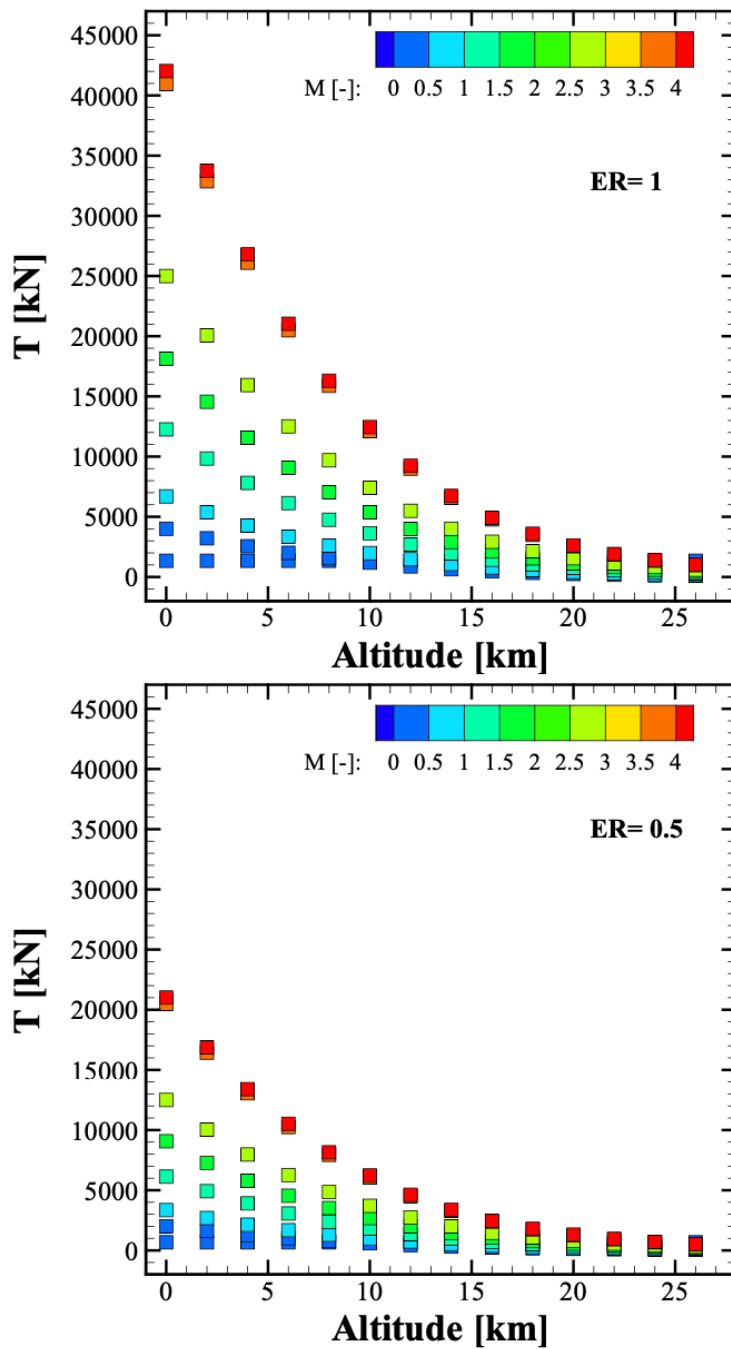


Figure 10 Net thrust of ATR as a function of flight altitude and Mach number as used in ASTOS [6]

As shown in previous charts, if the altitude remains constant, the higher is the Mach number, the higher is net thrust because it is a function of mass flow rate. On the other hand, if the speed flow remains constant and the altitude increases, the net thrust decreases, because of the mass flow drop.

Finally, there is a difference between ERs, that's because of net thrust dependency.

The charts show as well a maximum mass flow of $\dot{m} = 1050.68 \text{ kg/s}$ at $M=4.5$ and 0 km altitude but these conditions are never reached during the mission. Real flight conditions display maximum $\dot{m} = 100\text{kg/s}$.

DMR Propulsion modeling

DMR model is not that different from ATR one [6]. It is evaluated for altitudes from 18 to 40 km, speed flow from 4.5 to 8 Mach, ER=0.5 and ER=1, and AoA= -2° , 0° , $+2^\circ$. In this scenario, AoA influences the results, and on the contrary, if ER=0, any evaluation is not needed because net thrust and mass flows are equal to zero.

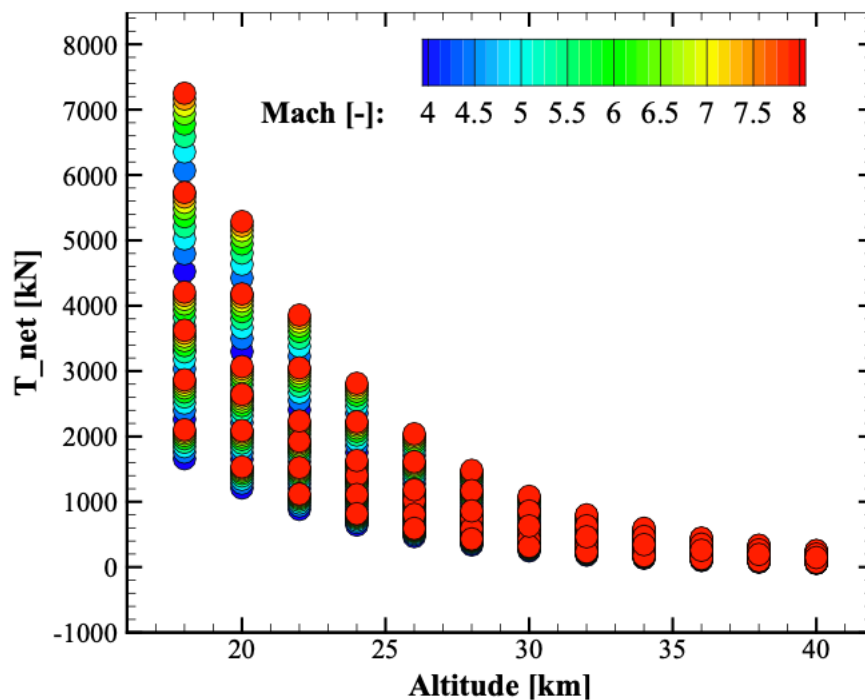


Figure 11 Net thrust of DMR as a function of flight altitude and Mach number as used in ASTOS [6]

As shown in the previous chart, every set is evaluated six times: three AoA and two Ers. It displays a similar trend to the ATR ones.

Maximum mass flow is $\dot{m} = 395.12 \text{ kg/s}$, and it is evaluated for minimum AoA (-2°), maximum flow speed ($M=8$), at 18km altitude, and ER=1. Real flight conditions display maximum $\dot{m} = 50\text{kg/s}$.

1.4 Aerodynamics

In order to develop this new aircraft concept, many different models and characteristics have been evaluated to satisfy every aspect of the mission. Particularly, a careful assessment on different flight regimes is required in order to shape a suitable for civil passenger transportation system able to fly from subsonic to a hypersonic speed. In order to do so, maximum aerodynamics efficiency is required to increase the performance and reduce fuel consumption and environmental impact. Specifically, intake performance are particularly crucial to minimize the interaction of the flow path with external and internal surfaces, to avoid additional drag [8].

Aerodynamics modeling

LAPCAT aerodynamics is utilized by STRATOFLY too, so the performances studied in previous reports will stand [6].

The factors which influence both drag and lift coefficients are flow speed and AoA, while dynamic pressure has effects only on the drag.

The vehicle can be considered a material point coincident with CoM, so aerodynamic moment coefficient and aerodynamic surfaces deflection are not implemented.

For this operation reference area and length are $A_{ref}=2365 \text{ m}^2$ $L_{ref}=94 \text{ m}$.

CD is evaluated for AoA= $-2^\circ, +2^\circ$, speed flow from 0.3 to 8 Mach and from 10,000 to 50,000 Pa dynamic pressure. This last variable shows how CD is related to a viscous component.

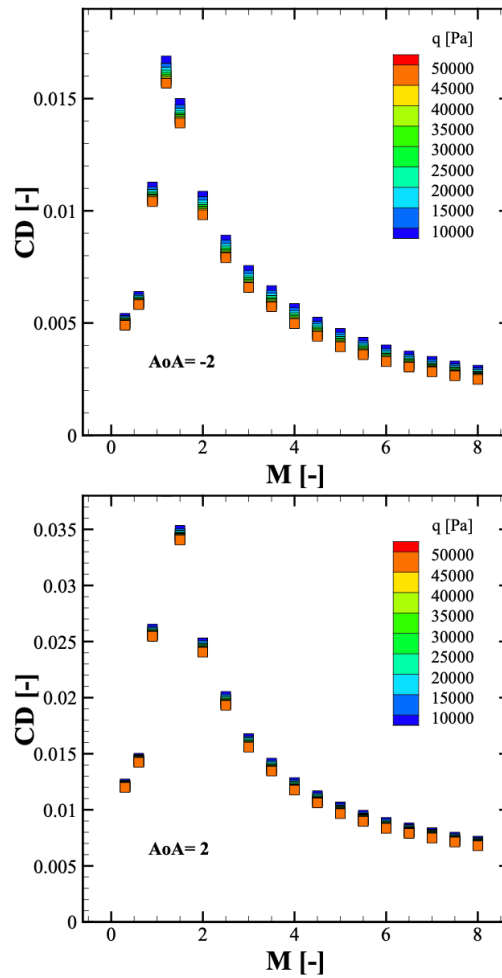


Figure 12 Drag coefficient used in ASTOS for different angle of attack as a function of Mach number and dynamic pressure [6]

As shown in the previous charts CD has the typical shape: rising with the speed since touching the top at $M=1$, then descending. It is also clear how CDs are lower for the negative AoA, they are almost half of the positive ones.

The same evaluation is reported for CL: AoA= -2° , 0° , $+2^\circ$, and flow speed from 0.3 to 8 Mach. However, in this scenario, CL must be corrected with a negative contribution due to flow spillage.

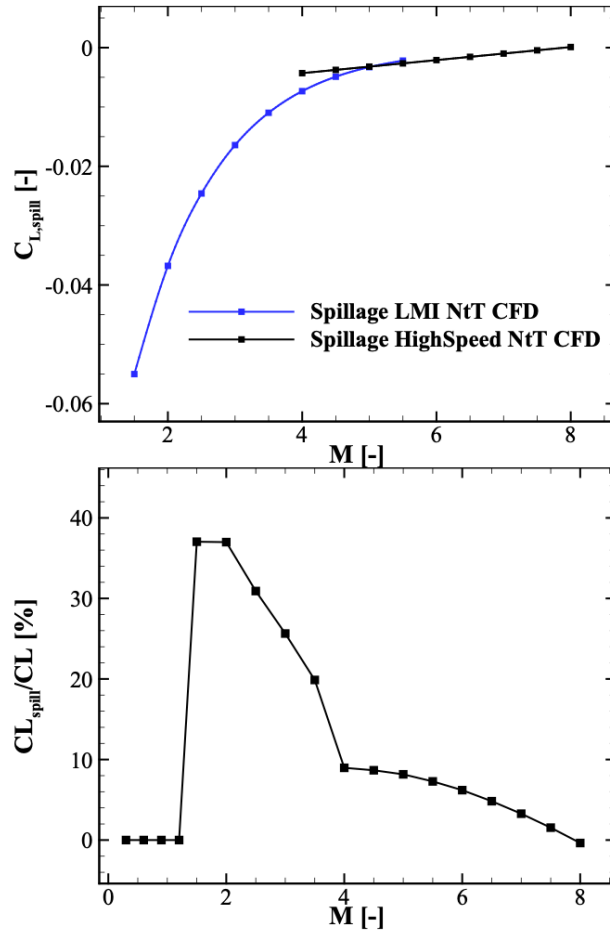


Figure 13 spillage drag coefficient as a function of Mach number (top) and spillage drag as a percentage of the vehicle lift (bottom) [6]

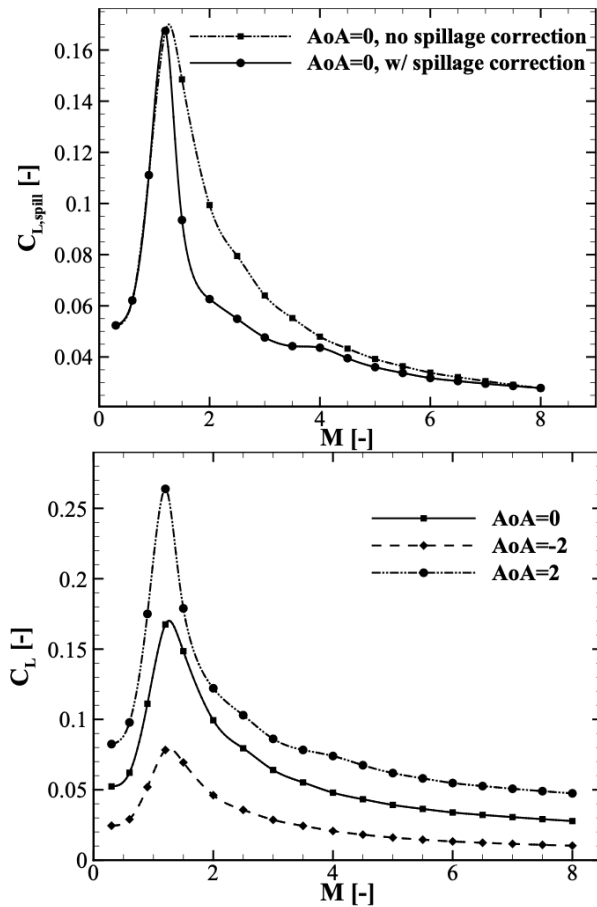


Figure 14 Lift coefficient with and without correction for spillage (top) and lift coefficient as a function of angle of attack (bottom) [6]

As shown in the charts, under $M=1$ there is no significant spillage. It reaches its maximum at $M=1.5$, then decreases.

1.5 Thermal Protection Subsystem

The Thermal Protection Subsystem (TPS) job is to protect the aircraft from external extreme heat flux generated at hypersonic speed. TPS follows two principal models: passive and active.

The passive one protects the aeroshell from the heat using an insulating material such as ceramics. These kinds of materials are not good heat conductors, so the aircraft is isolated from the external environment.

The active method collects part of the heat with pipes under the aeroshell and conducts it towards the tanks to boil the fuel necessary for the Thermal and Energy Management Subsystem.

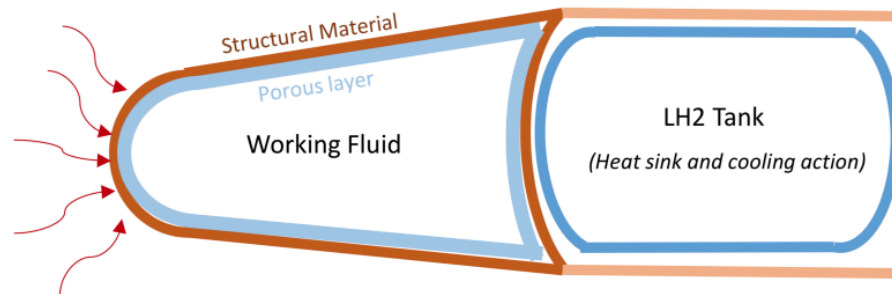


Figure 15 Active Thermal Protection Subsystem model

1.6 Thermal and Energy Management Subsystem

Dealing with high temperature and high heat load due to hypersonic flight is not that easy. For this reason, different methods and techniques have been studied, developed, and embedded as Thermal and Energy Management Subsystems (TEMS). There is a tight cooperation between TPS, TEMS, and the Environmental Control and Life Support Subsystem (ECLSS).

TEMS duty is to manage the high temperatures coming from the TPS and collect the heat load also from other subsystems.

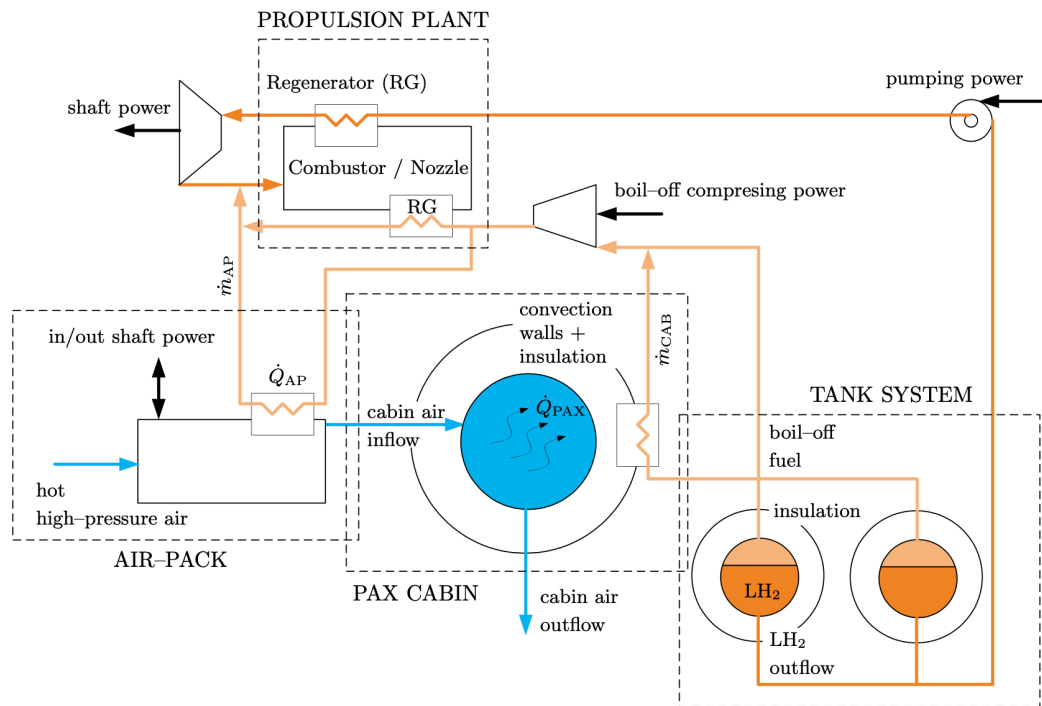


Figure 16 Thermal and Energy Management System model [12]

As shown in the model, the aerodynamic heat is collected through the aeroshell by the TPS. It is conducted to the tanks where LH₂ is stocked at T=20 K. The heat boil LH₂ off and, after an appropriate cycle, it can be used in two different ways. H₂ gas helps ECLSS to cool the cabin, while the other part is compressed and injected into the combustion chamber, being used as a coolant at the end of the cycle [12] [13].

Chapter 2

Statistical analysis

This chapter analyzes statistically all the re-entry vehicles exploiting a configuration that can be considered similar to the one of STRATOFLY MR3 and studies their aerodynamics coefficients, in order to obtain average CL, CD, L/D vs Mach shapes to be used as inputs for the Matlab code utilized to study the re-entry corridor.

1.1 Space Shuttle [14]

The Space Shuttle is a semi-reusable concept for the transportation of payloads and passengers up to low Earth orbit (LEO), about 200 km.

It is composed of three elements:

- Two solid rockets booster;
- One external tank;
- Orbiter vehicle.

The Space Shuttle was launched using a ramp, and at an altitude of 50 km (about 120 s) there was the separation of the boosters, they were recovered in the ocean. At 110 km the tank was expelled, all the maneuvers and the deorbiting were operated by the Orbital Maneuvering System, at last, the re-entry was unpowered.

The Space Shuttle was quite versatile, its missions were carrying heavy payloads in orbit, including some International Space Station (ISS) segments, transporting passengers, satellites, and even parts of the Hubble Space Telescope.

The Space Shuttle was involved in two disasters: Challenger (1986) and Columbia (2003).

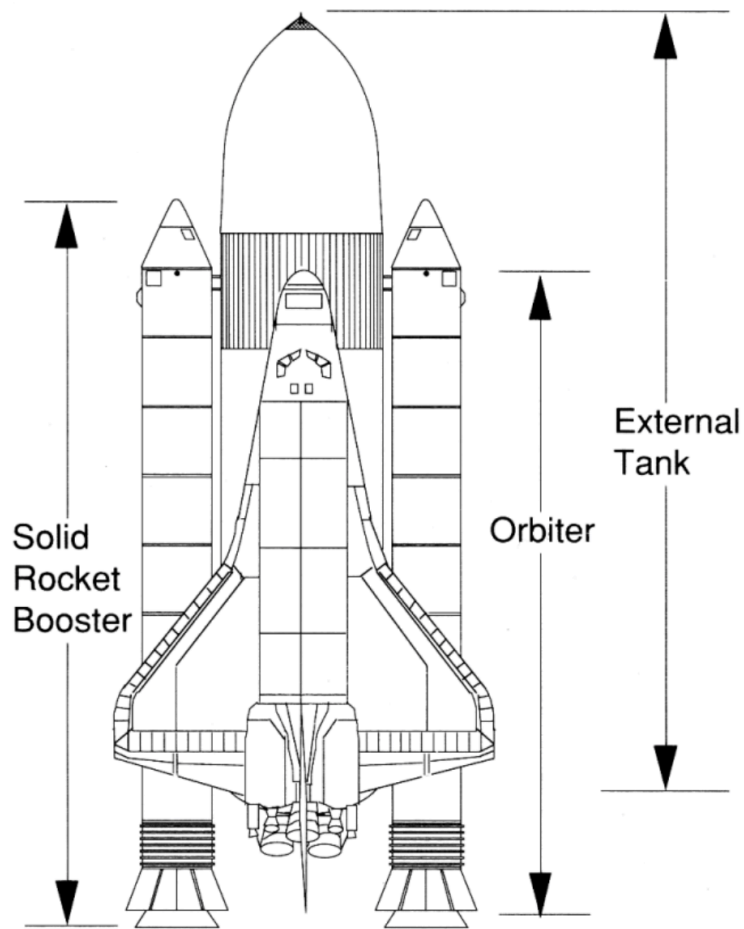


Figure 17 Space Shuttle Configuration [14]

Space Shuttle design

The Space Shuttle was the biggest space vehicle ever built. Its characteristics are reported as follows

total length	L_{tot}	37.238 m
total width	W_{tot}	23.842 m
reference length	L_{ref}	32.774 m
reference area	S_{ref}	249.909 m ²
reference chord length (M.A.C.)	c^-	12.060 m
x-coordinate of the center-of-gravity, nominal	x_{cog}	27.348 m \Rightarrow 0.65 L_{ref} Fig. 6.3
z-coordinate of the center-of-gravity, nominal	z_{cog}	9.525 m Fig. 6.3

empty mass	me	78 000 kg
gross mass at launch	mg	110 000 kg
double delta sweep angle	α	81° - 45°

Table 1 SPACE SHUTTLE Orbiter shape: dimensions, quantities, and reference values [14]

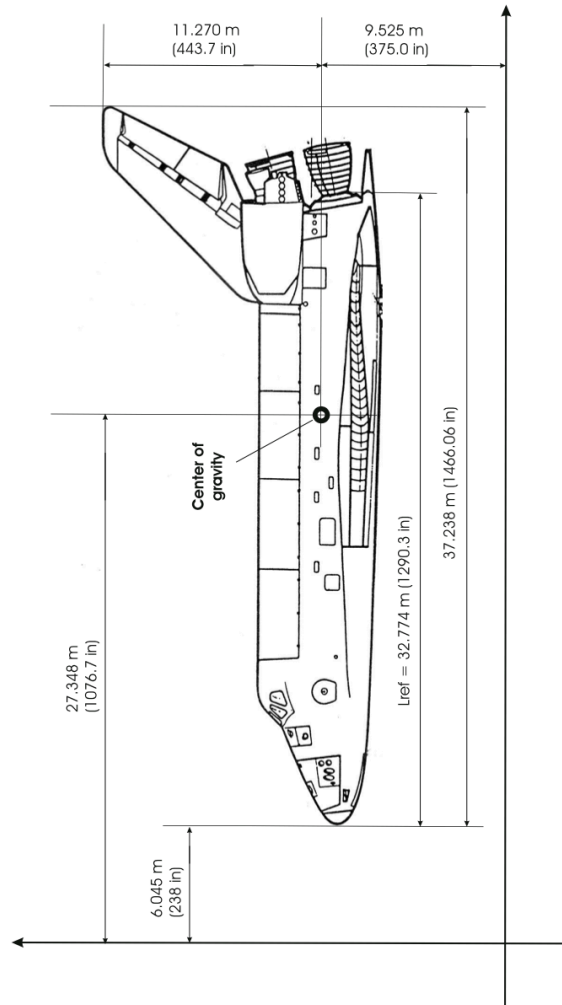


Figure 18 Shape definition of the SPACE SHUTTLE Orbiter [14]

Space Shuttle Aerodynamics

The following charts show the aerodynamic coefficients, and efficiency in subsonic, transonic, supersonic, and hypersonic conditions.

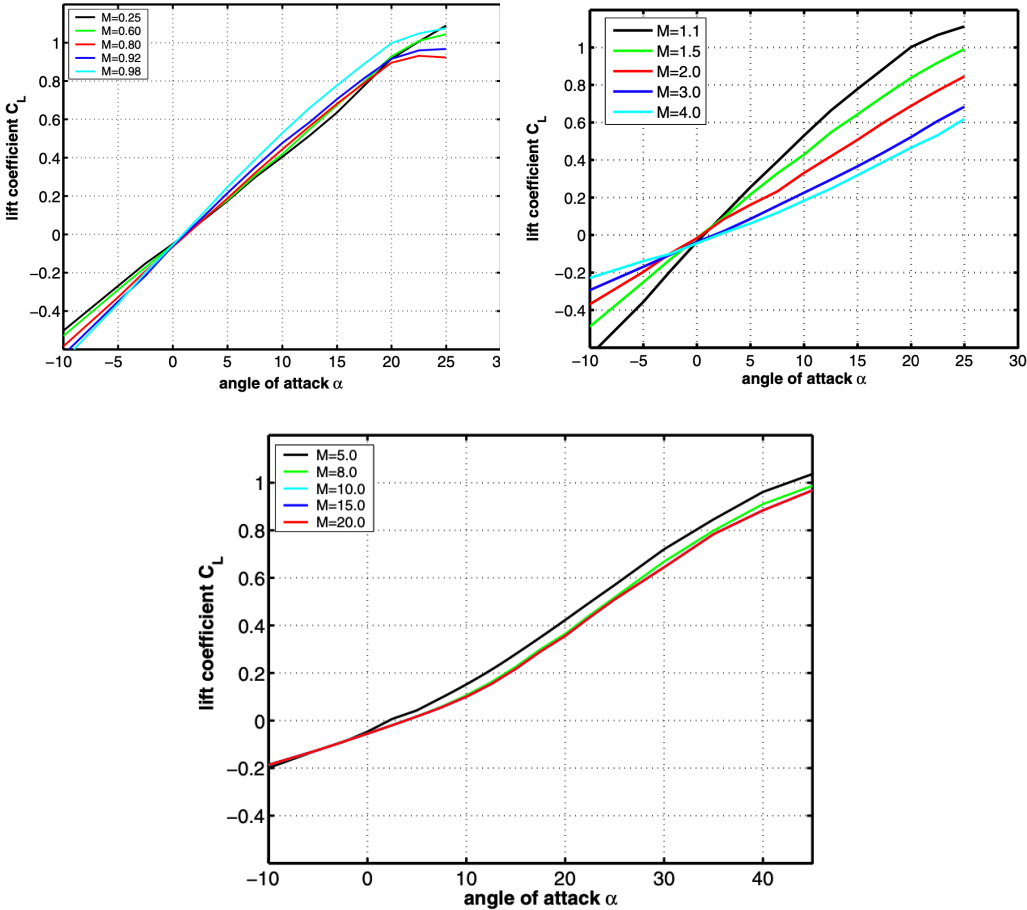


Figure 19 Lift coefficient C_L as function of the angle of attack α for subsonic, transonic-supersonic, and hypersonic Mach numbers [14]

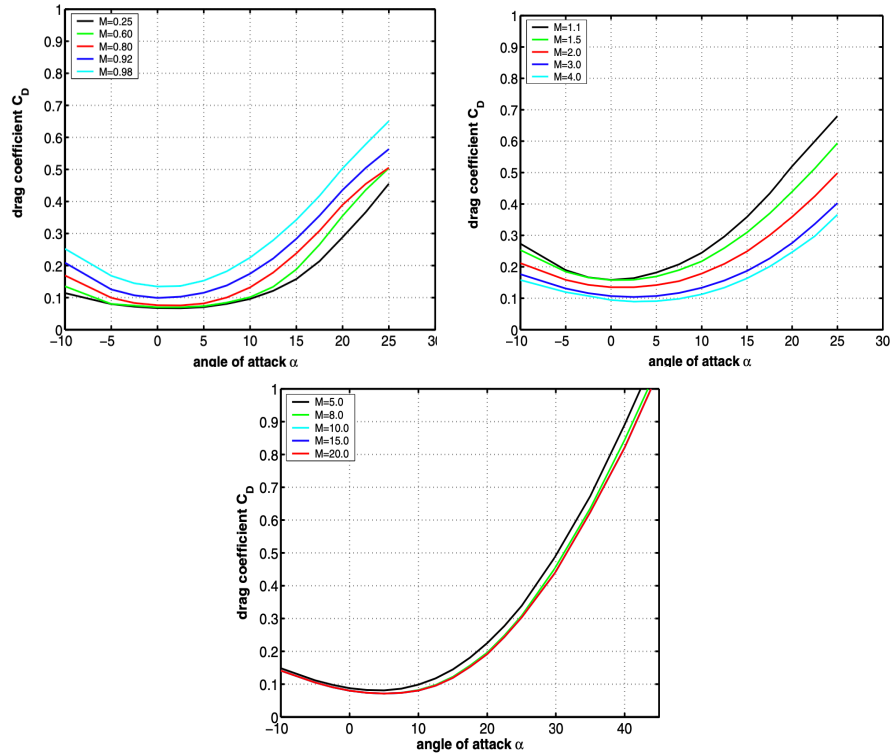


Figure 21 Drag coefficient C_D as function of the angle of attack α for subsonic, transonic- supersonic, and hypersonic Mach numbers [14]

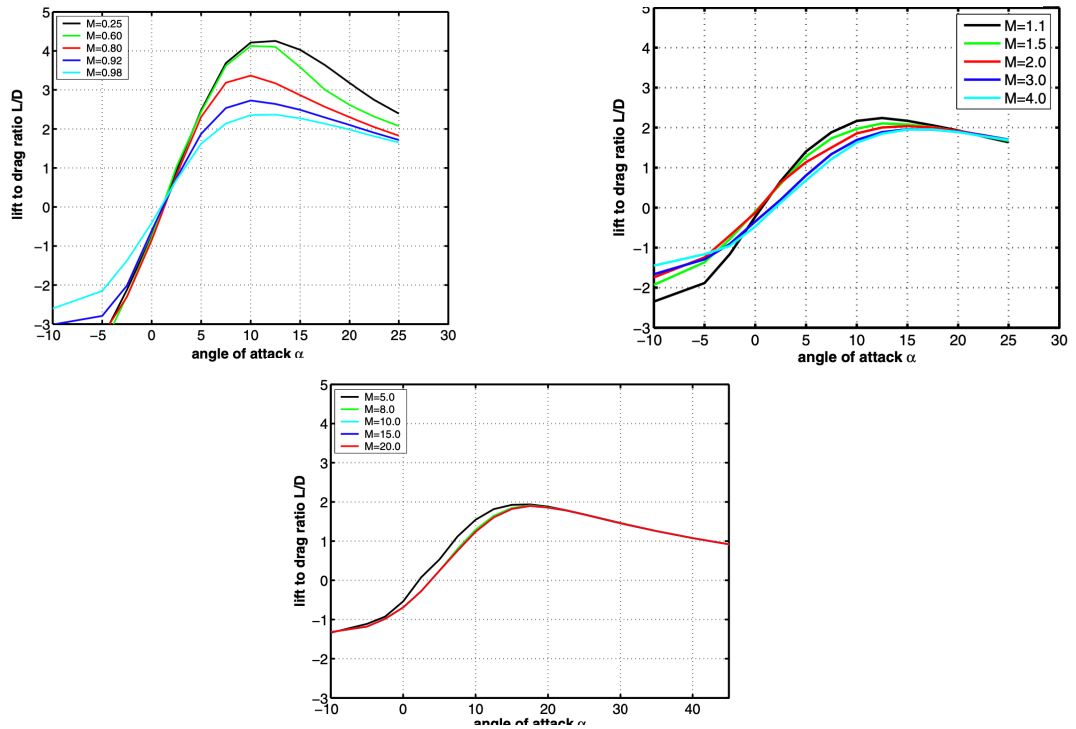


Figure 20 Efficiency as function of the angle of attack α for subsonic, transonic- supersonic, and hypersonic Mach numbers [14]

2.2 X-33 [14] [15]

X-33 should have been Space Shuttle heir, launched in 1996, it was a winged body vehicle capable of carrying payloads and human passengers.

To reduce costs of semi-reusable Space Shuttle configuration, X-33 was designed as a fully reusable vehicle (RLV) single-stage-to-orbit (SSTO), capable of a vertical launch and a conventional landing.

The program was shut down in 2001.

X-33 design

X-33 had a delta-winged body shape with two dihedral canted fins and it had aerospike engines powered by liquid oxygen and hydrogen.

reference length	$L_{ref} = 19.3 \text{ m (63.2 ft)}$
reference area	$S_{ref} = 149.4 \text{ m}^2 \text{ (1608 ft}^2\text{)}$
pitching moment reference point	$x_{ref} = 12.71 \text{ m (41.7 ft)} \Rightarrow 0.66 L_{ref}$

Table 2X-33 shape: dimensions, quantities, and reference values [14]

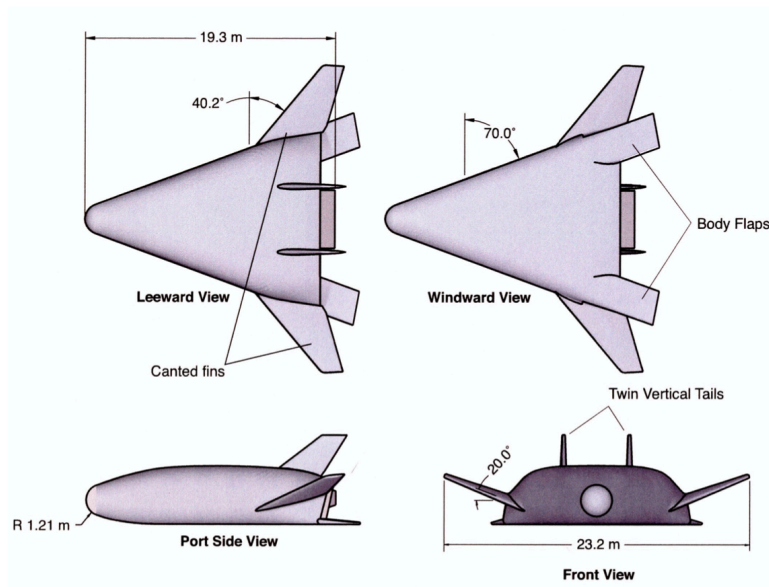


Figure 22 Shape definition of the X-33 [14]

X-33 Aerodynamics

The following charts show the aerodynamic coefficients, and efficiency in subsonic, transonic, supersonic, and hypersonic conditions.

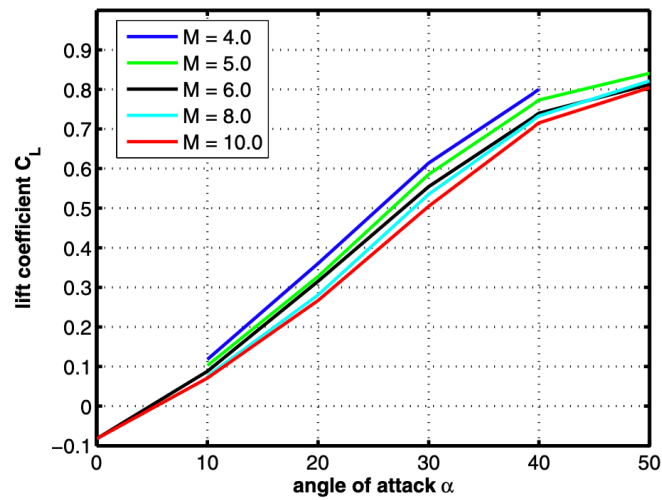


Figure 23 Lift coefficient C_L as function of the angle of attack α for subsonic, transonic- supersonic, and hypersonic Mach numbers [14]

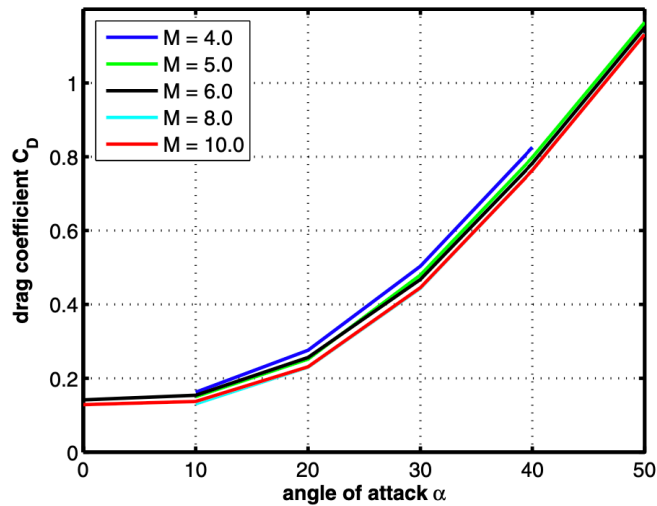
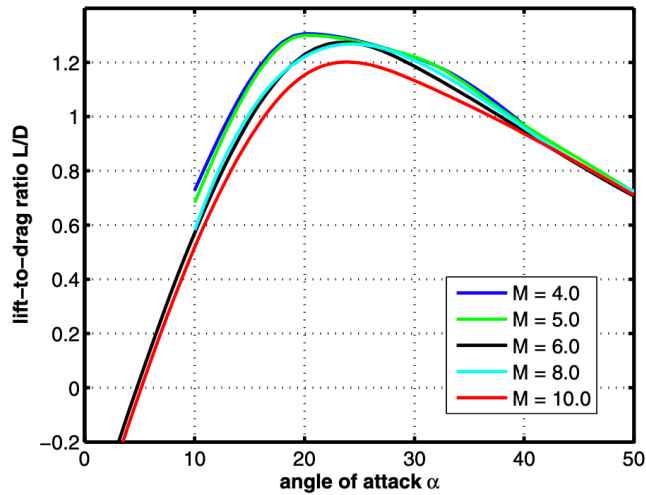


Figure 24 Drag coefficient C_D as function of the angle of attack α for subsonic, transonic- supersonic, and hypersonic Mach numbers [1]



3.3 X-34 [14] [15]

X-34 is the third demonstrator vehicle developed by Orbital Science Corporation. It was a test to implement new technologies:

- lightweight primary and secondary composite structures,
- reusable composite propellant tanks,
- advanced thermal protection system (TPS),
- flush air data system,
- integrated low-cost avionics using differential Global Positioning System (GPS),
- autonomous flight and landing.

X-34 maximum speed was $M=8$ and it reached 76 km altitude. The demonstrator used to be launched from an L-1011 carrier at $M_\infty = 0.7$ employing new low-cost engines.

The program was shut down in 2001 due to massive costs.

X-34 design

X-34 design was similar to the Space Shuttle Orbiter, with double delta wings.

reference length	$L_{ref} = 646.9 \text{ in. (16.43 m)}$
reference width	$B_{ref} = 332.9 \text{ in. (8.45 m)}$
reference height	$L_{ref} = 142.2 \text{ in. (3.61 m)}$
reference area	$S_{ref} = 357.5 \text{ ft}^2 (33.21 \text{ m}^2)$
moment reference point	$x_{ref} = 420 \text{ in. (10.67 m)} \Rightarrow 0.65 L_{ref}$
double delta sweep angle	$80^\circ - 45^\circ$

Table 3X-34 shape: dimensions, quantities, and reference values [14]

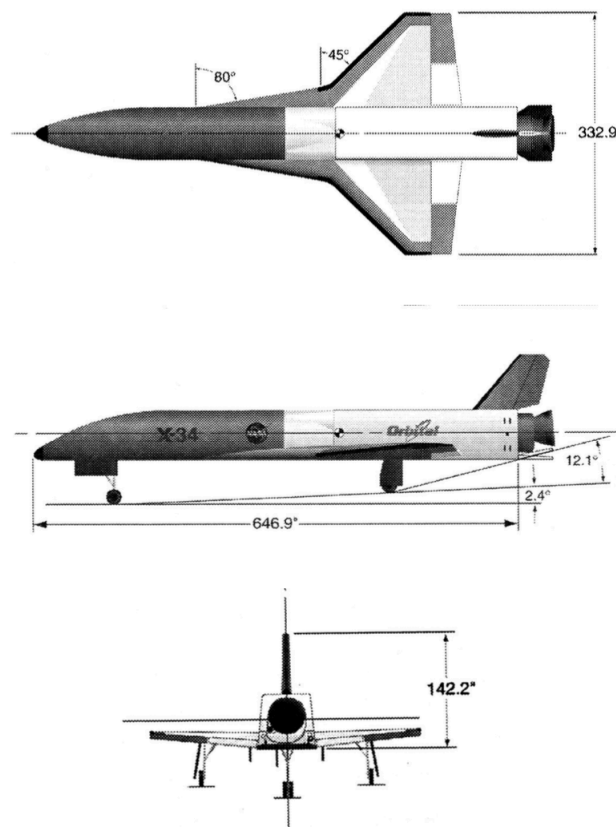


Figure 25 Shape definition of the X-34 [14]

X-34 Aerodynamics

The following charts show the aerodynamic coefficients, and efficiency in subsonic, transonic, supersonic, and hypersonic conditions.

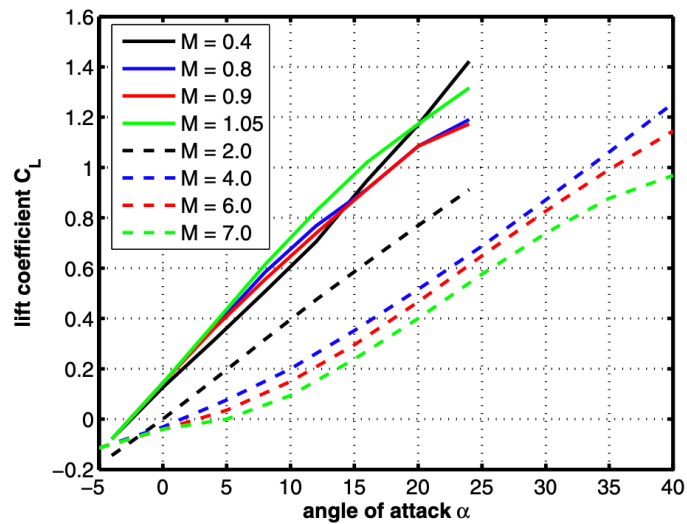


Figure 26 Lift coefficient C_L as function of the angle of attack α for subsonic, transonic- supersonic, and hypersonic Mach numbers [14]

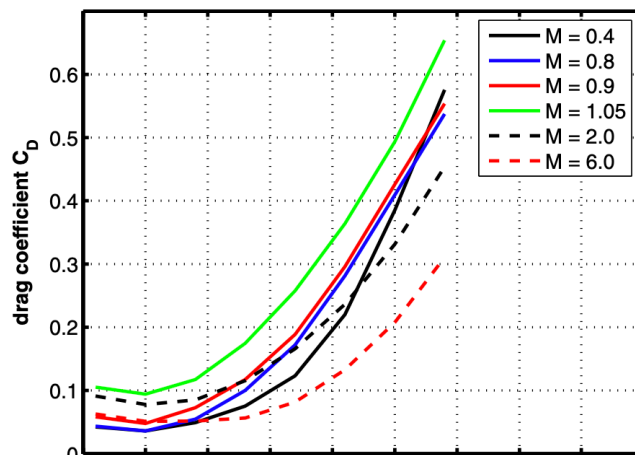


Figure 27 Drag coefficient C_D as function of the angle of attack α for subsonic, transonic- supersonic, and hypersonic Mach numbers [14]

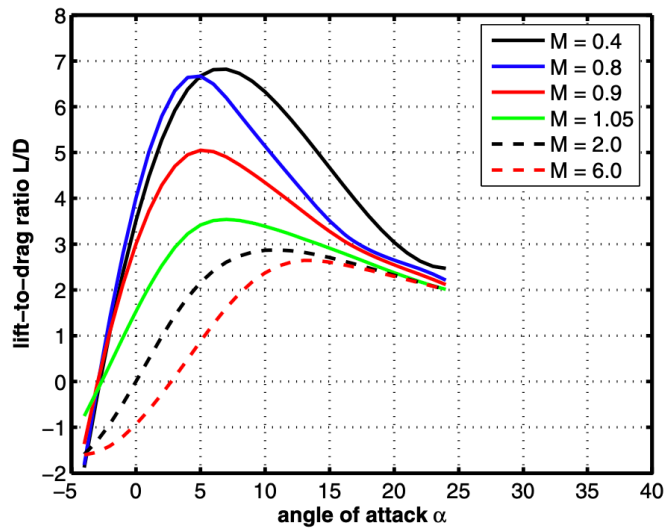


Figure 28 Efficiency as function of the angle of attack α for subsonic, transonic- supersonic, and hypersonic Mach numbers [14]

4.2 Hope-X [14]

Hope was a Japanese project of reusable vehicle. Its mission was to transport payload and passengers to the ISS.

In 1990 the project was re-oriented, due to the lack of funds, into a smaller, lighter, cheaper, and unmanned vehicle, Hope-X

Hope-X design

Hope-X had double delta wings, similar to the Space Shuttle Orbiter, but it also had a winglet at the wing tips. This configuration was born out of cooperation between German and Japanese space agencies.

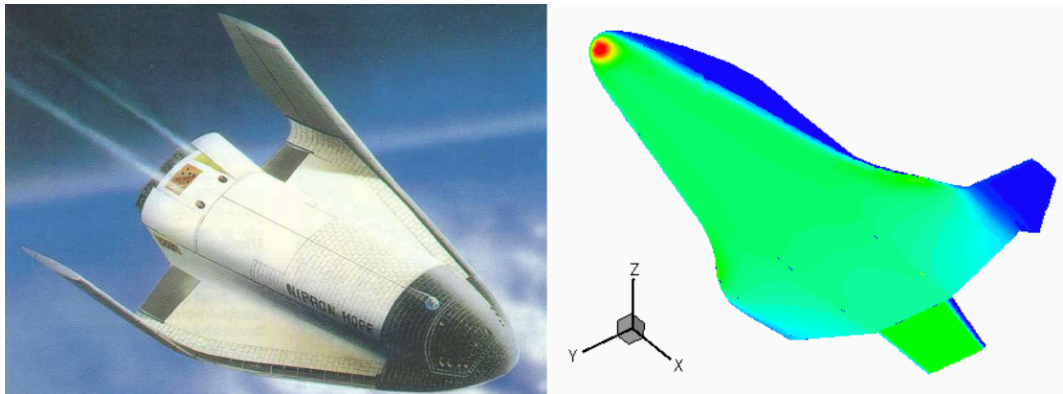


Figure 29 HOPE-X shape: synthetic image (left), surface pressure distribution for $M_\infty = 3$ and $\alpha = 35^\circ$ (right) [14]

Hope-X aerodynamics

The following charts show the aerodynamic coefficients, and efficiency in subsonic, transonic, supersonic, and hypersonic conditions.

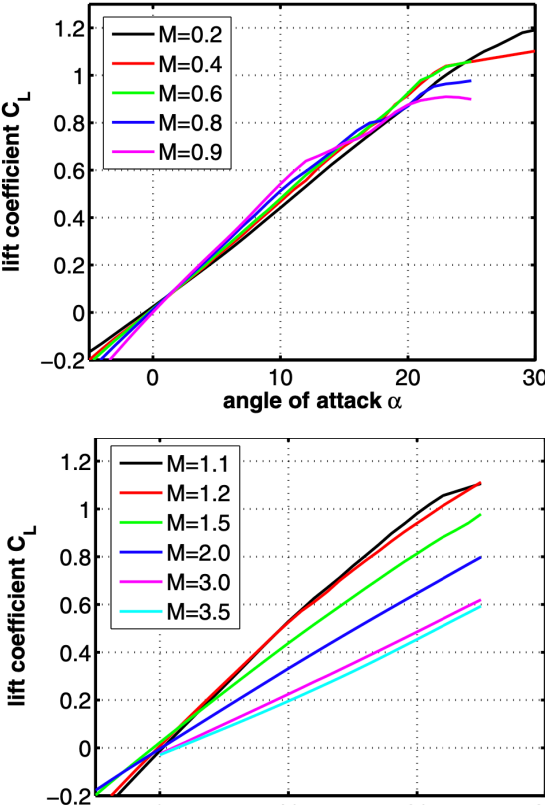


Figure 30 Lift coefficient C_L as function of the angle of attack α for subsonic (top) and supersonic Mach (bottom) [14]

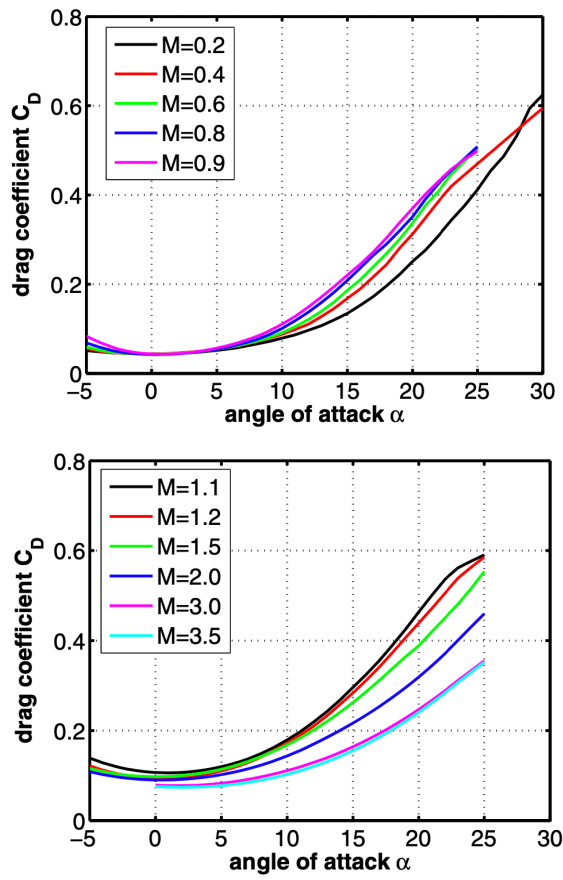


Figure 31 Drag coefficient C_D as function of the angle of attack α for subsonic (top) and supersonic Mach (bottom) [14]

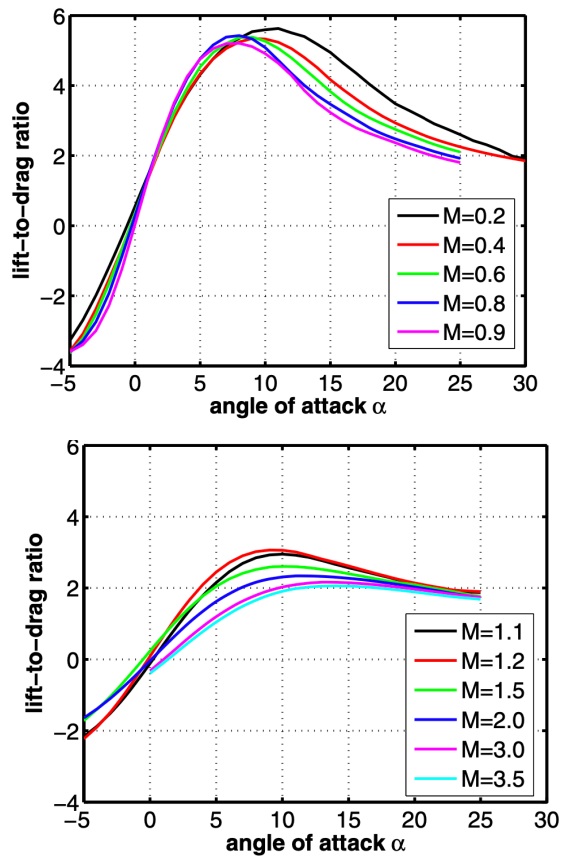


Figure 32 Efficiency as function of the angle of attack α for subsonic (top) and supersonic Mach (bottom) [14]

5.2 Hermes [14] [16]

During the space race, France proposed to the European Union the construction of an innovative vehicle capable to compete with American and Russian ones. So, in November 1987, the European Space agency started the Hermes program, an innovative completely reusable winged vehicle. Its main features were:

- ascent to low Earth orbit (up to 800 km) on top of the ARIANE V rocket;
- 30-90 days mission duration in orbit;
- total launch mass 21000 kg;
- fully reusability;

- initially, the transportation of six astronauts and 4 500 kg payload into low Earth orbit, and after a reorientation a reduction to three astronauts and a transportation payload of 3000 kg.

In 1993 the program was shut down due to the end of the cold war and massive cost. No vehicle was ever built, just wind tunnel experiments and CFD models.

Hermes design

Hermes was projected with a delta wing with a 74° sweep angle and winglet on the tips.

The design of this vehicle was very different from the Space Shuttle Orbiter and way more innovative. The Shuttle had problems with lateral stability because, due to the high angle of attack on the re-entry path, the rudder was in the hypersonic shadow and it wasn't aerodynamically effective until 30km of altitude. This problem was solved by implementing a new kind of rudder installed on the winglets, in this way lateral capability was obtained already at 70 km of altitude.

total length	L _{tot}	14.574 m
total width	W _{tot}	9.379 m
reference length	L _{ref}	15.500 m
reference area	S _{ref}	84.67 m ²
x-coordinate of center-of-gravity	x _{cog}	8.722 m Fig. 6.153
empty mass	m _e	15 000 kg
gross mass at launch	m _g	21 000 kg

Table 4 Hermes shape: dimensions, quantities, and reference values [14]

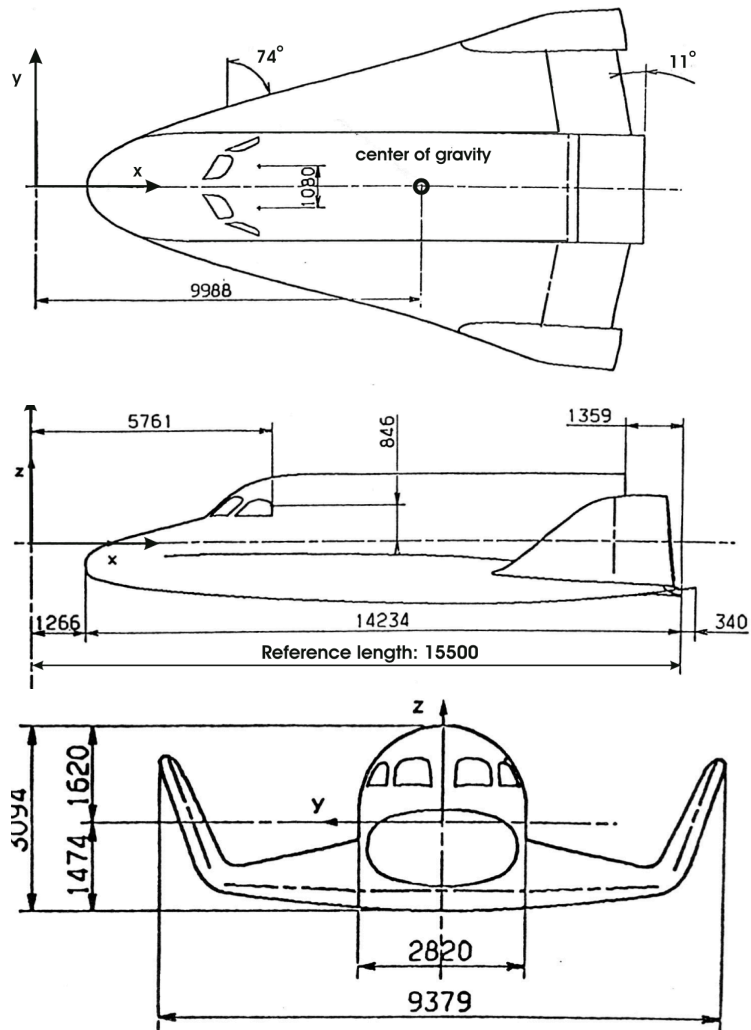


Figure 33 Hermes design definition [14]

Hermes aerodynamics

The following charts show the aerodynamic coefficients, and efficiency in subsonic, transonic, supersonic, and hypersonic conditions.

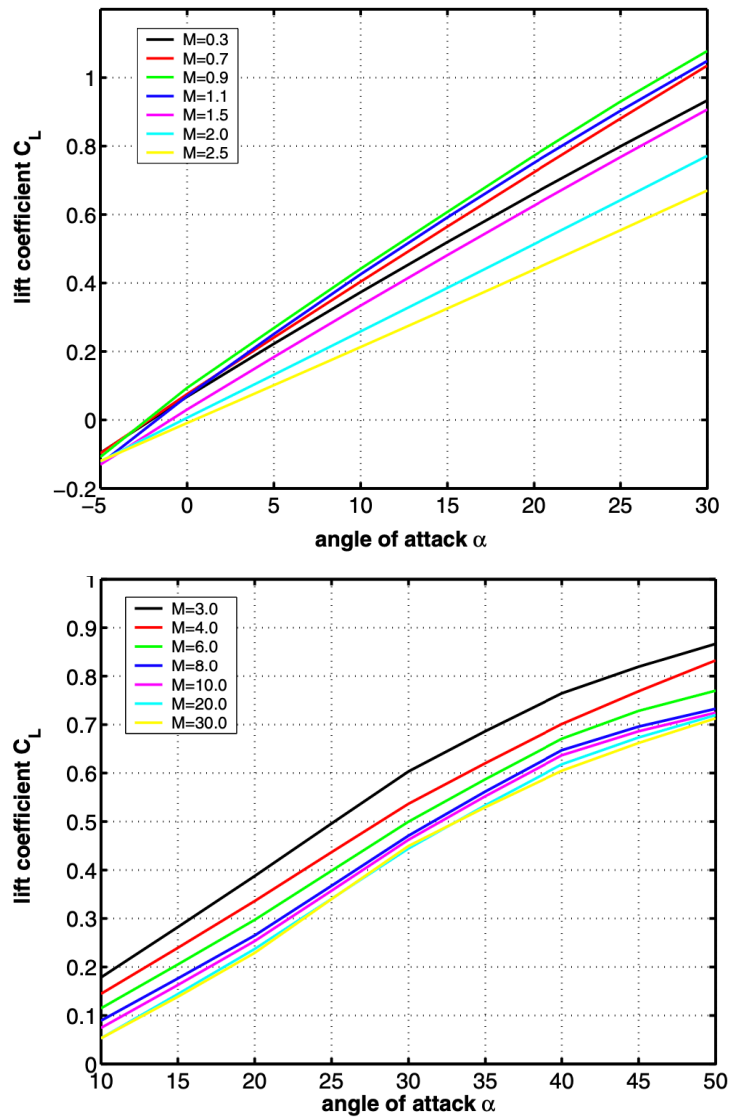


Figure 34 Lift coefficient C_L as function of the angle of attack α for subsonic (top) and supersonic and hypersonic Mach (bottom) [14]

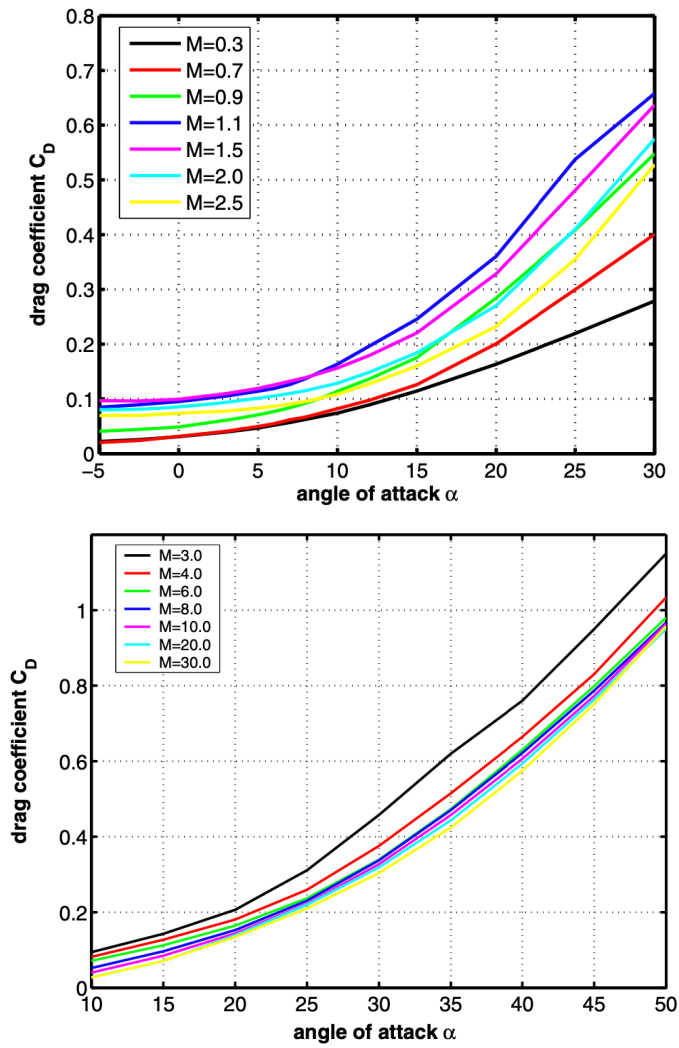


Figure 35 Drag coefficient C_D as function of the angle of attack α for subsonic (top) and supersonic and hypersonic Mach (bottom) [14]

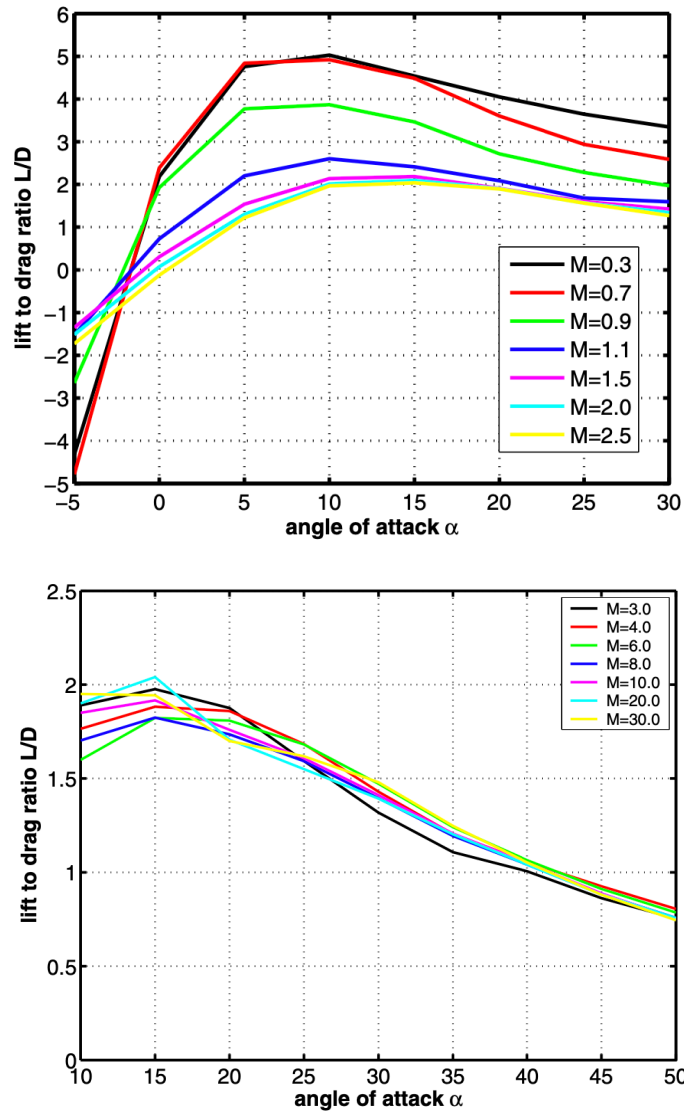


Figure 36 Efficiency as function of the angle of attack α for subsonic (top) and supersonic and hypersonic Mach (bottom) [14]

6.2 Sänger and Horus [14] [17]

Saenger was the result of a German program born in 1988 which aimed to find a new innovative solution for access to space without using conventional expensive rockets. The idea was a partially reusable vehicle, similar to the Space Shuttle system. The reference concept was a Two-Stage-To-Orbit system (TSTO). Eugen Sänger was the first engineer to suggest this kind of solution in 1963, that's why the project is named after him.

The Two-Stage-To-Orbit system is a spacecraft capable of taking off and landing like a conventional plane. The first stage climbs till the separation altitude, then the second proceeds to the operational altitude.

Saenger consisted of a lower and an upper stage, named Horus.

The engineers studied two different mission scenarios: the first one was the lower stage taking the upper Horus, positioned in a trough on the back, to 33 km altitude, leaving him climbing to Earth orbit, the second was to evaluate it as a hypersonic passenger aircraft. The European Hypersonic Transport Vehicle (EHTV) derives from this second setup.

Saenger design

Saenger was designed with a double delta wing with a small negative dihedral angle. The total length of the vehicle amounts to 82.4 m, its span width is 45.2 m.

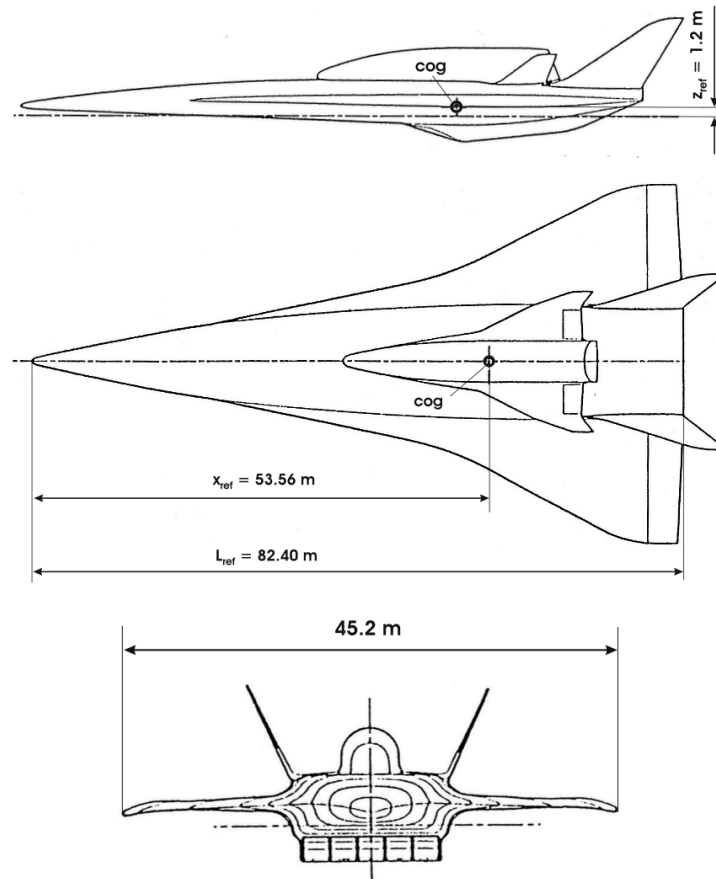


Figure 37 Saenger design definition [14]

Saenger aerodynamics

The following charts show the aerodynamic coefficients, and efficiency in subsonic, transonic, supersonic, and hypersonic conditions.

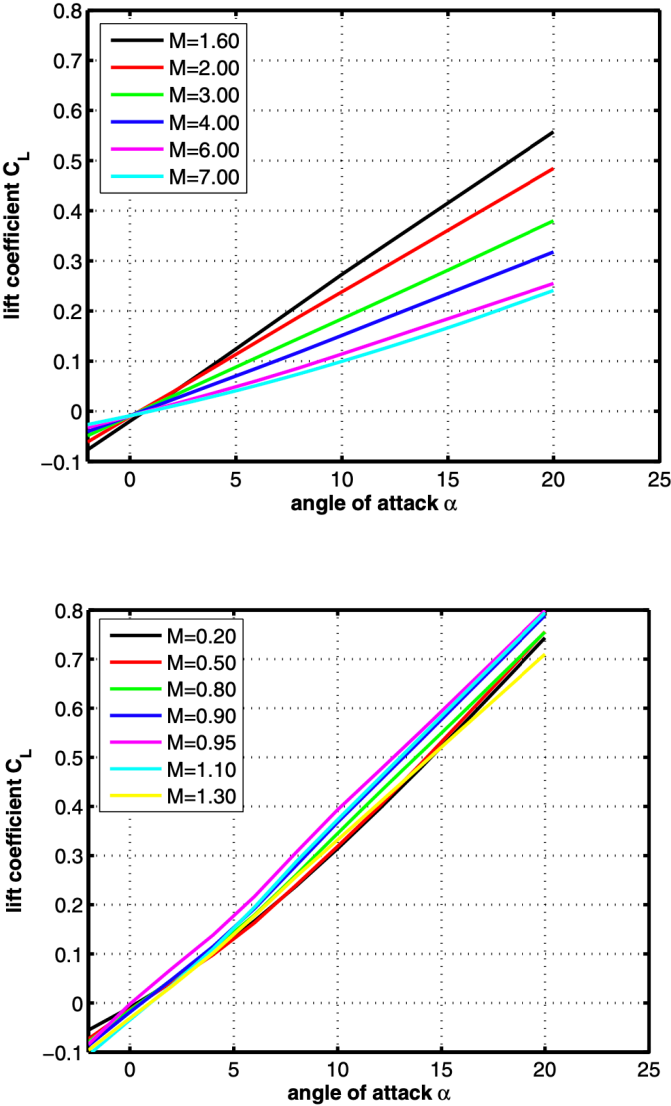


Figure 38 Lift coefficient C_L as function of the angle of attack α for subsonic (top) and supersonic and hypersonic Mach (bottom) [14]

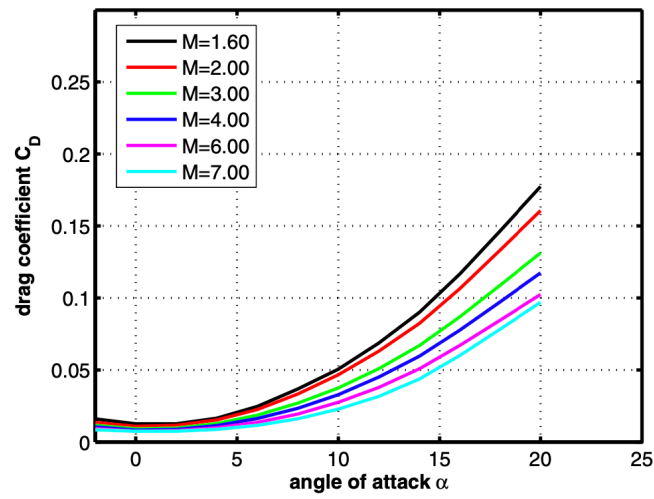
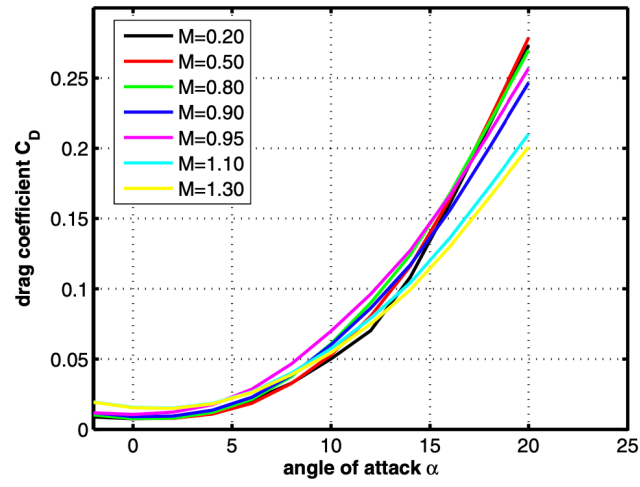


Figure 39 Drag coefficient C_D as function of the angle of attack α for subsonic (top) and supersonic and hypersonic Mach (bottom) [14]

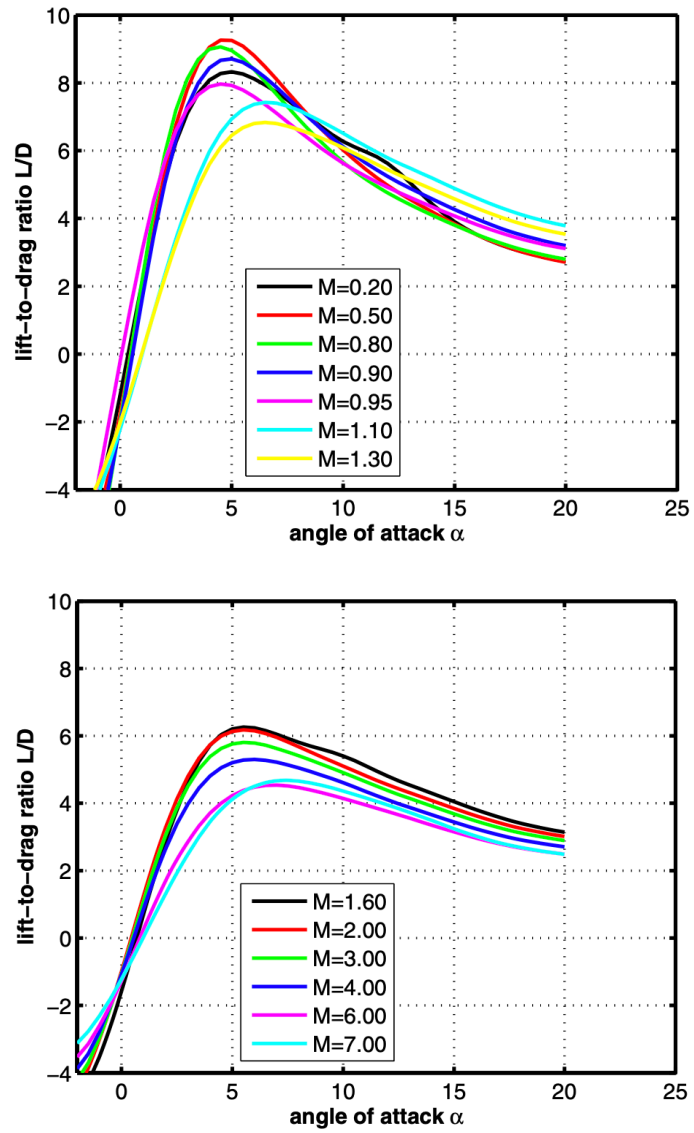


Figure 40 Efficiency as function of the angle of attack α for subsonic (top) and supersonic and hypersonic Mach (bottom) [14]

6.3 Conclusions

Collecting all the data, these are the statistical results elaborated by Matlab.

Lift Coefficient

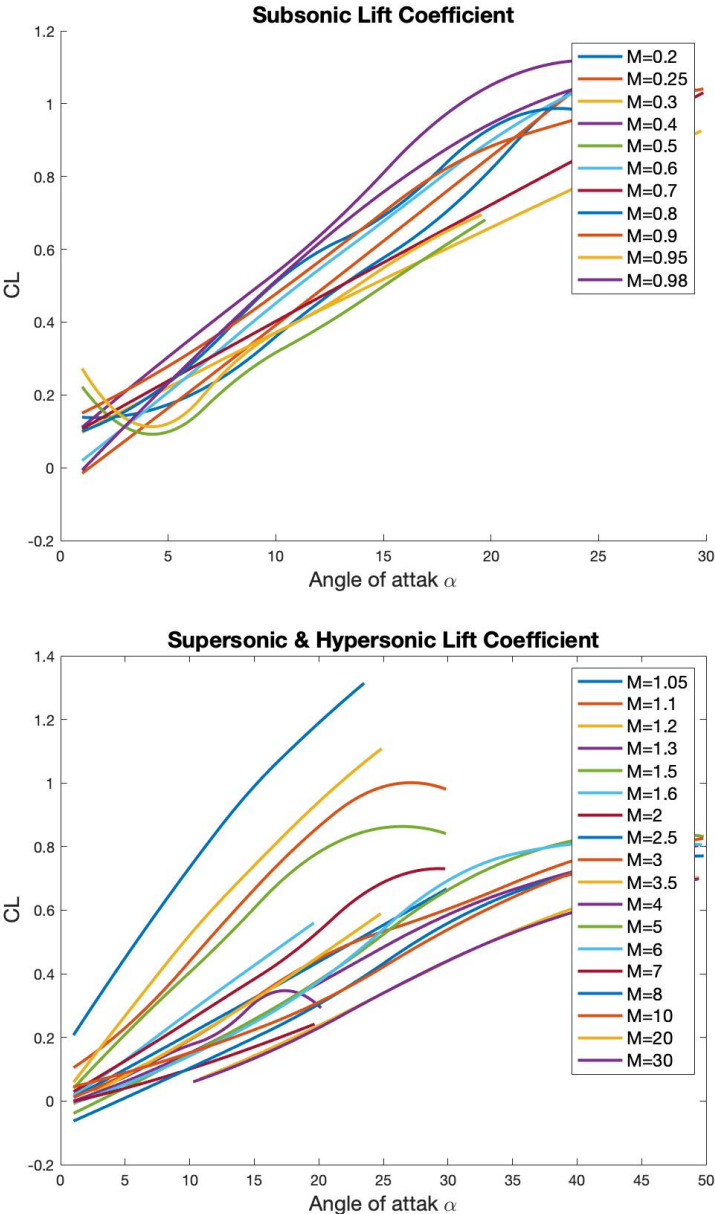


Figure 41 Lift coefficient CL as function of the angle of attack α for subsonic (top) and supersonic and hypersonic Mach (bottom)

Drag Coefficient

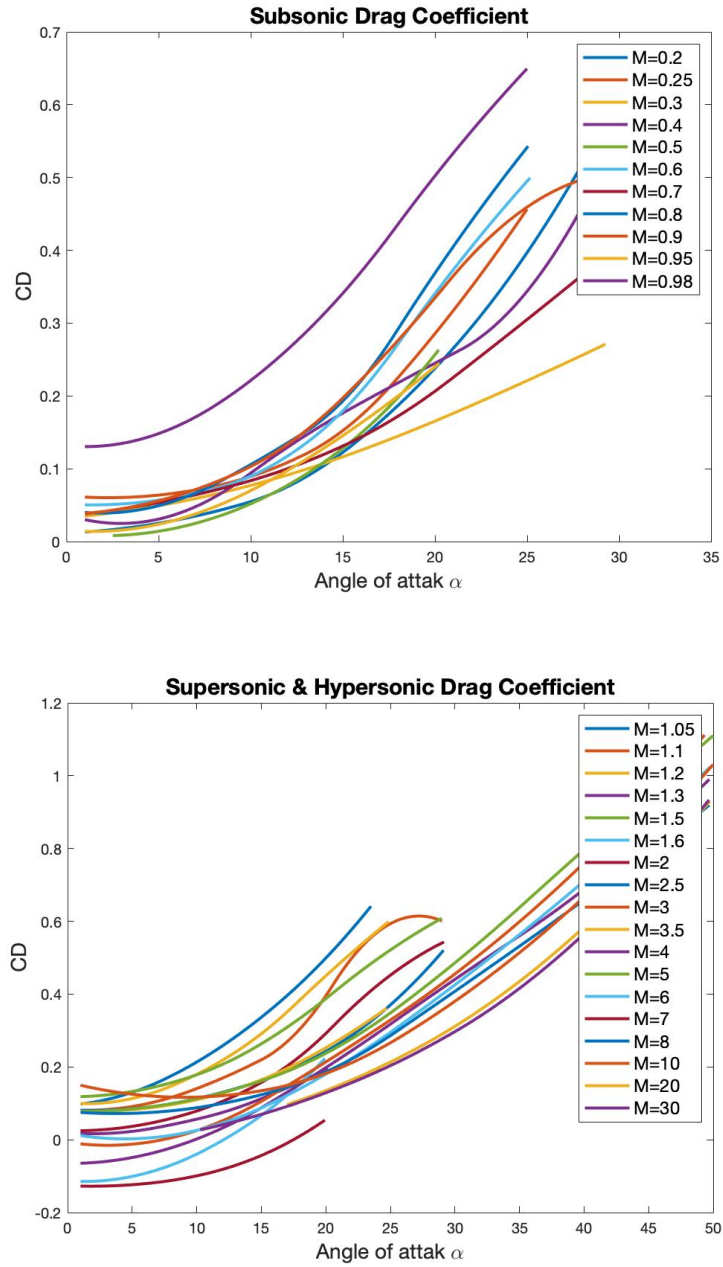


Figure 42 Drag coefficient CD as function of the angle of attack α for subsonic (top) and supersonic and hypersonic Mach (bottom)

Efficiency

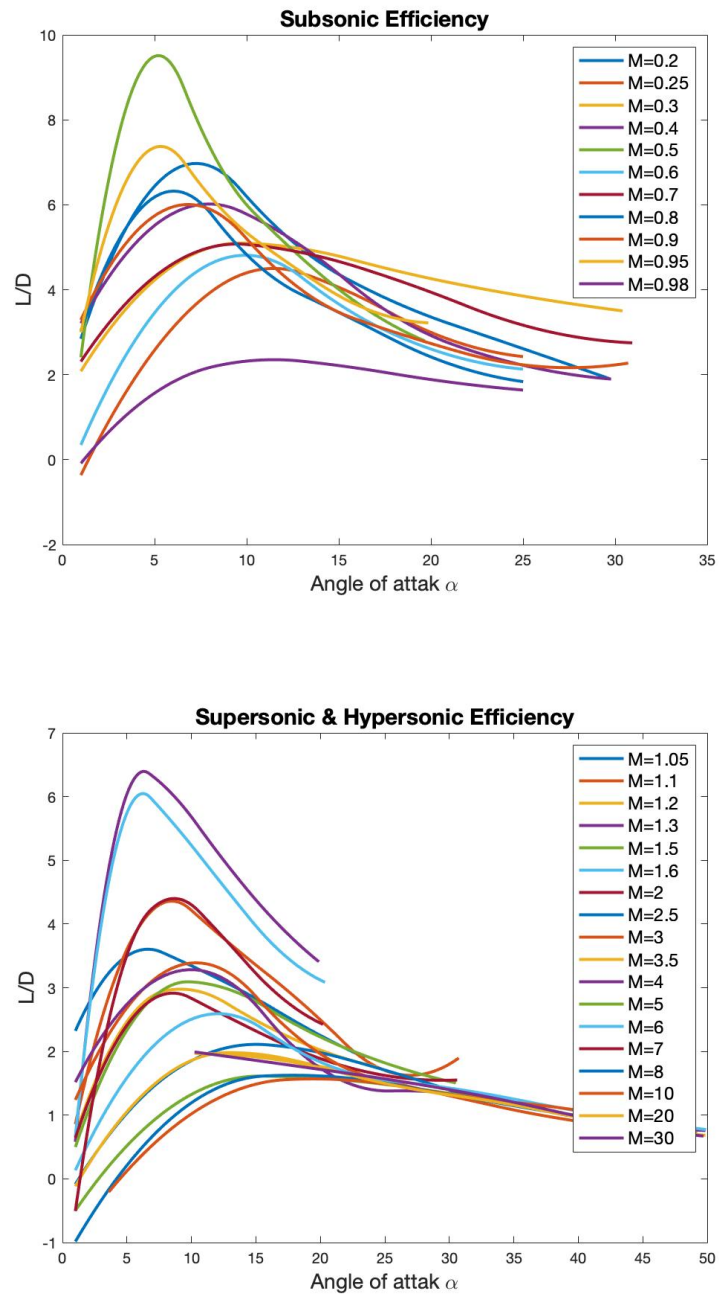


Figure 43 Efficiency as function of the angle of attack α for subsonic (top) and supersonic and hypersonic Mach (bottom)

Chapter 3

Atmospheric Re-Entry

3.1 Introduction

This work considers to exploit STRATOFLY MR3 vehicle as first stage of a TSTO system. To perform its mission, STRATOFLY MR3 will fly across the stratosphere. On the other hand, the second stage will be launched during high-speed flight leg, reaching then the required target orbit. Afterwards, on its descending phase, it will deal with the atmosphere re-

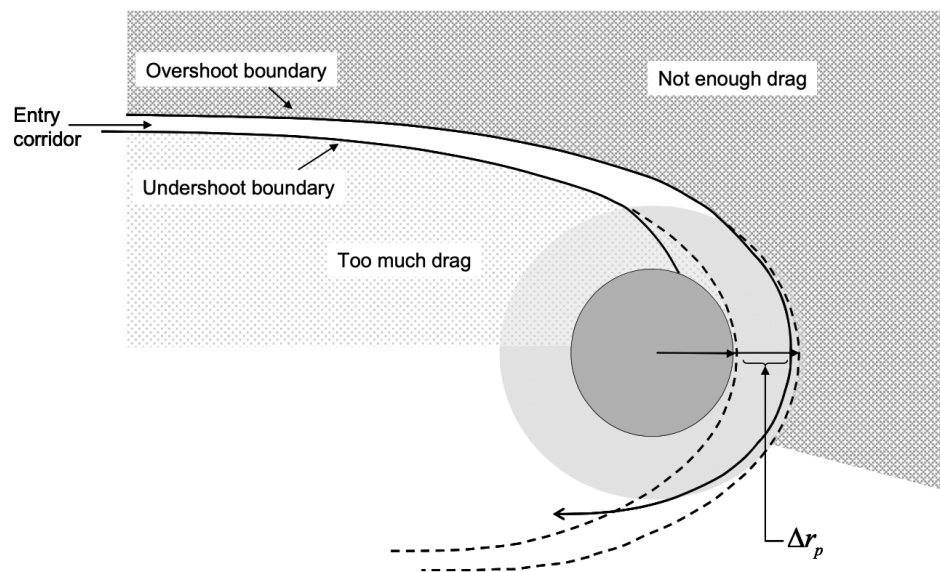


Figure 44 Entry corridor [21]

entry. This delicate moment needs balance between competing requirements: deceleration, heating, and accuracy. Excessive deceleration could damage the structure of the aircraft, such as the vulnerable hinges, its payload, or the passengers. The human body can tolerate up to 12 Earth g's, but since for passengers comfort, a value of about 3 Earth g's would be more suitable. On the other hand, too little deceleration can cause a bounce on the atmosphere.

Heat strongly restricts the operational aircraft capability. It is generated due to the interaction between the structure and the atmosphere and it is dangerous for heating loads and heating rates.

These constraints build a tiny three-dimensional entry corridor where the aircrafts can fly safely, it is less than 0.1° .

In short, if there is too little drag the aircraft bounces off the atmosphere and it's called overshoot, if the drag is too much, the heat or the g-load is too heavy and it's called undershoot.

3.2 Entry Corridor

The entry corridor is defined by the constraints and it is the area where the aircraft can fly safely.

The entry corridor defines the trajectory's constraints and indicates where it's safe descending. The nominal flight profile is the ideal pathway to follow and it's in the middle of the corridor to ensure that if any accidents occur, it doesn't affect the descent.

The best way to study all these constraints is to find performance-invariant quantities, which define deceleration, heating, range, and cross-range capability. Those quantities are the lift-drag ratio (L/D) and the ballistic coefficient ($\beta=m/CDS$). The width of the corridor depends principally on the first one, for this reason, a statistical study on aerodynamics characteristics was carried out in the previous chapter.

The ability to change attitude during the flight is crucial because it allows to improve the aircraft performances by exploiting changing the speed during the descent. By increasing the angle of attack near CD_{max} in the early high-speed phase, peak heat rate is minimized, lowering it at $(L/D)_{max}$ during the lower-speed phase maximizes range and cross-range.

The second stage of the STRATOFly TSTO system is supposed to be a winged reusable vehicle, therefore its (L/D) is expected to be high and it allows to have full attitude control. The bank angle (Φ) controls directly the direction of the lift vector and this controls the drag acceleration and vehicle guidance. Rolling the aircraft lift-down increases the drag acceleration, rolling the aircraft lift-up and the vehicle accelerates out of the

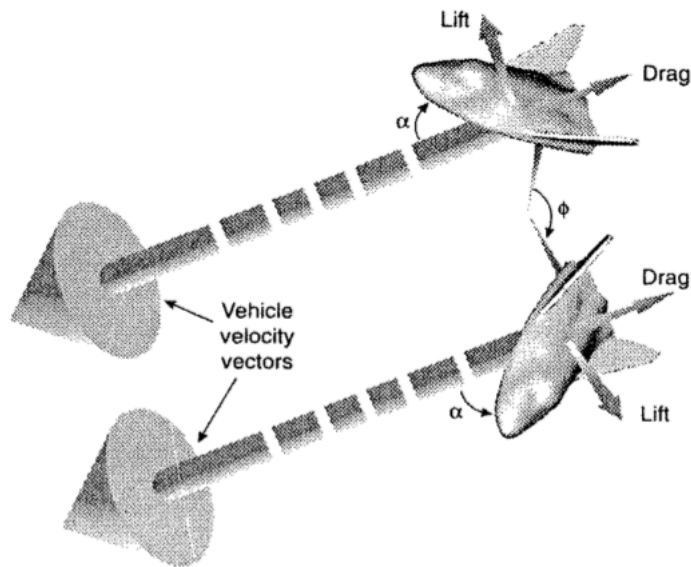


Figure 45 Aerodynamic bank maneuver [19]

atmosphere, reducing the drag acceleration.

A big (L/D) has side effects too:

- higher heat rates on sharp sections;
- higher design complexity;
- reduce volumetric efficiency because the center of pressure has to be located after the aircraft center of mass to have longitudinal stability.

3.3 Constraint Boundaries

In a chart, the entry corridor is an area defined by the intersections of lines that represent the boundaries. Two different charts can show the entry corridor. The first one has on the x-axis the speed and on the y-axis the altitude, the second one, which is reported in this dissertation, has on the x-axis the speed and on the y-axis the drag acceleration.

Heating peak, dynamic pressure, acceleration are the load constraints that define the upper boundaries. The saturation limit for trajectory control of equilibrium glide is the lower constraint.

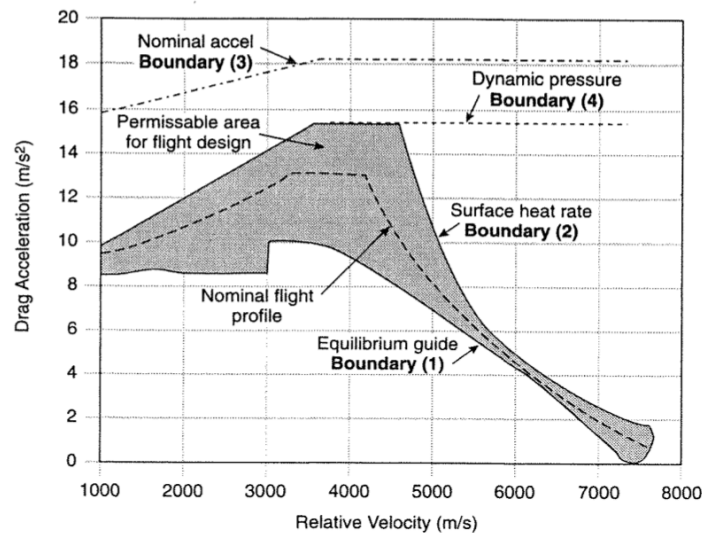


Figure 46 Re-entry Corridor [19]

Boundary 1: Constraint on equilibrium glide

“The physical basis is that in gliding flight the vertical component of the acceleration tends to be small, and the flight path angle is likely to be small” [18]. The equilibrium glide enables the aircraft to have a consistent range and cross-range. The constraint defines the minimum drag profile that allows the lifting vehicle to fly at quasi-constant altitude.

The banking angle defines the aircraft roll attitude and the direction of the lifting vector. If only a portion of the lift balances the gravity, the remaining part allows the vehicle to maneuver, if the lift is barely enough to balance the gravity, the maneuverability is lost and the aircraft is not able to proceed towards the desired target.

Boundary 2: Constraint on heat rate

The constraint on heat rate is determined by the structural design of the vehicle and its performance to managed it. That’s why it is important to

design properly the Thermal Protection Subsystem and the Thermal and Energy Management Subsystem.

Not observing this constraint, the subsystems can't manage the heat and it endangers the structural integrity of the vehicle, just like happened with the Space Shuttle disaster.

The proper choice of material is crucial to prevent excessive heating rate peaks, if they are $>125 \text{ W/cm}^2$, ablative materials are requested.

However, this constraint takes into consideration just the convective heating loads generated by the friction with the atmosphere, leaving the radiative heat.

Boundary 3: Constraint on total sensed acceleration

The total sensed acceleration affects the passengers and the aircraft structure. It is constant at fixed (L/D), but changes with the vehicle attitude.

Boundary 4: Constraint on dynamic pressure

The dynamic pressure or moments generated by the re-entry speed on hinges of control surfaces can cause dramatic failures due to the lack of flying controls.

Nominal Flight Profile

The result of combining all the boundaries on a speed-drag acceleration chart is the operative area called re-entry corridor and the nominal flight profile is the best path to follow.

The nominal flight profile is sited in the middle of the corridor withstanding unexpected problems that can lead the aircraft outside the operational area and defines nominal range and cross-range.

Chapter 4

Matlab Model

4.1 Objectives

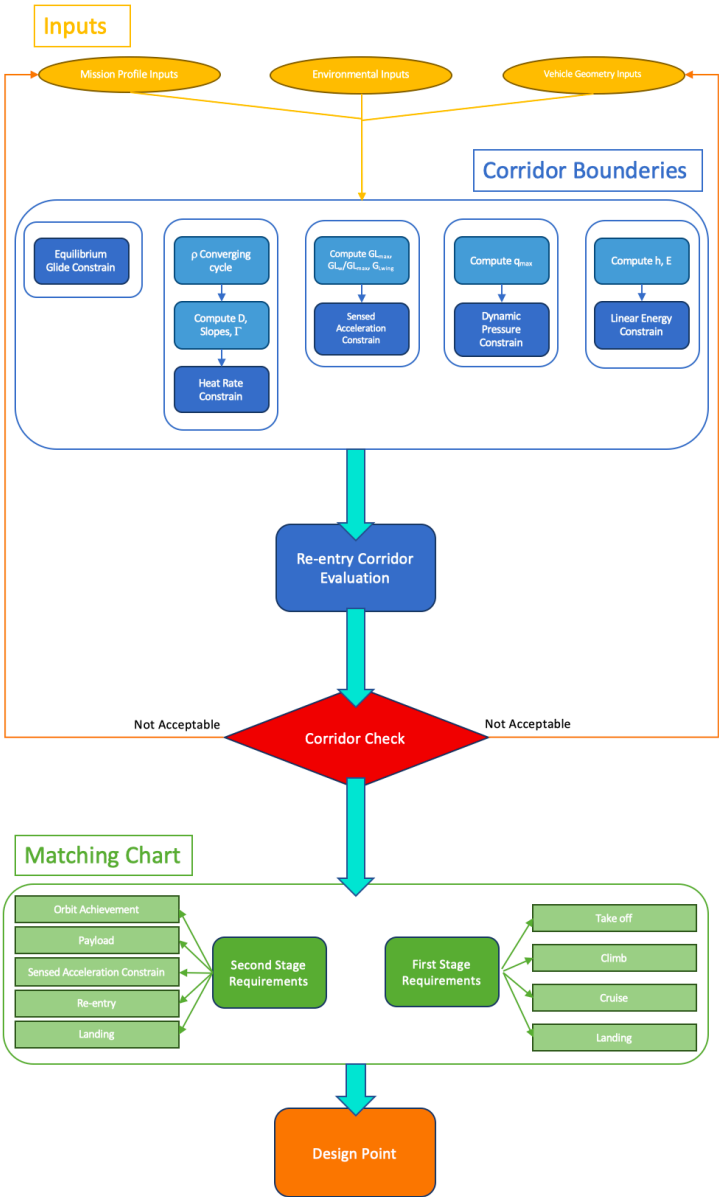


Figure 47 Matlab Flow Chart

The Matlab model built has these four objectives:

- it studies STRATOFLY TSTO system re-entry mission requirements and finds performance invariant quantities;
- analyzes how those quantities modify the re-entry corridor and the constraint boundaries;
- checks if a re-entry corridor is possible utilizing STRATOFLY TSTO system take-off outputs from previous studies;
- if there is no corridor, determines an optimization cycle that satisfies the requirements;
- provides a matching chart for the first and second stage.

4.2 Boundary Equation

Boundary 1: Constraint on equilibrium glide [19]

The equation that defines the equilibrium glide is

$$D_{ref1} = \left(\frac{g_0 \left(1 - \frac{v^2}{v_{sat}^2} \right)}{\frac{L}{D} \cos(\Phi_{min})} \right)$$

(4. 1)

g_0 is the gravitational constant [m/s²];

v is the local speed [m/s];

L/D is the lift-drag ratio given by the statistical analysis;

v_{sat} is the constant satellite circular velocity [m/s]

Φ_{min} is the minimum banking angle. the average minimum banking angle that it was taken into consideration is 30°.

It is possible to notice that if L/D increases, the vehicle can fly at lower drag acceleration during equilibrium glide, therefore higher L/D denotes a longer range, expanding aircraft footprint.

Boundary 2: Constraint on heat rate [19] [20] [16]

The way to find the heat constraint is an iterative cycle based on the Detra-Kemp-Riddel convective heat rate equation

$$qCons = qConst * \left(\frac{1}{R_n}\right)^{\frac{1}{2}} * \left(\frac{\rho_d}{\rho_0}\right)^{\frac{1}{2}} * \left(\frac{v}{v_{sat}}\right)^{3.15}$$

(4. 2)

qConst is a constant evaluated 11,030 on Earth;

ρ_0 is the density at sea level [kg/m³];

ρ_d is the local density [kg/m³];

Rn is the nose radius fixed as 0.3 m.

STRATOFly TSTO second stage is a fully reusable vehicle, therefore ablative materials are not used in its TPS, so the maximum heating rate must be <125 W/cm²;

The iterative cycle has several passages and at the end it defines the quadratic coefficient required by the drag reference.

$$D_{ref2} = \Gamma_1 + \Gamma_2 v + \Gamma_3 v^2$$

(4. 3)

Boundary 3: Constraint on total sensed acceleration [19]

A fixed value of total sensed acceleration determines a fixed drag acceleration, if the angle of attack remains constant, and so the L/D.

The equation that shows this relationship is

$$D_{ref3} = \Gamma_4 = D_{max} = \frac{G_{max}}{\sqrt{1 + \left(\frac{L}{D}\right)^2}}$$

(4. 4)

where G_{max} is defined as

$$G_{max} = v_e^2 \sin(\gamma_e) / (2e g_0 H_s)$$

(4. 5)

v_e is the atmospheric entry speed [m/s];

γ_e is the flight path angle [rad];

H_s is the planet atmosphere density scale [m].

However, a correction is necessary because the second stage here considered is a winged vehicle, so

$$\frac{G_L}{G_{max}} = \frac{g_0 e^{\left(\frac{2\gamma_e}{L/D}\right)}}{L/D}$$

(4. 6)

Boundary 4: Constraint on dynamic pressure [19]

Drag-acceleration for the dynamic constraint is defined as

$$D_{ref4} = \frac{Q_{max}}{\beta}$$

(4. 7)

Q_{max} is the constraint on dynamic pressure 14.3 kPa;

β is the ballistic coefficient defined as

$$\beta = \frac{m}{CD * S}$$

(4. 8)

m is the aircraft mass [kg];

CD is the drag coefficient;

S is the cross-sectional area.

Boundary 5: Profile for linear drag

When the vehicle reaches the desired acceleration limit, it starts the constant drag-acceleration phase, cutting speed, and heat load.

The more velocity decreases the more the flight angle increases, so the small approximation is not valid anymore. To simplify hypersonic equations avoiding integrating the range equation occurs an exchange of variables from velocity to speed. In this way, given the final target energy value, initial and final velocity, and initial and final drag values, the linear drag profile is defined.

$$h_{i,f} = h_0 - h_s * \ln\left(\frac{2 * D_{i,f} * \beta_{i,f}}{v_{i,f}^2 * \rho_0}\right)$$

(4. 9)

$D_{i,f}$ is the initial or final drag acceleration;

$$E_{i,f} = g_{i,f} * h_{i,f} + \frac{v_{i,f}^2}{2}$$

(4. 10)

$$\Gamma_5 = (D_i - D_f)/(E_i - E_f)$$

(4. 11)

$$D_{ref5} = D_f + \Gamma_5 * (E - E_f)$$

(4. 12)

4.3 Performance Invariant Quantities

Analyzing the equation of the previous section at first glance several variables influence them.

Looking at the first equilibrium glide equation, two seem to be the key factors, L/D and deorbit altitude. If L/D rises, the drag-acceleration tends to move down, just like if the bank angle decreases. On the other hand, if the deorbit altitude increase, the boundary tends to be flatter.

The maximum heat rate is fixed because of the reusable nature of the vehicle and by its structure.

In the total sensed boundary equation, if L/D and operational altitude increase, the drag-acceleration decreases. The same result is obtained if the flight path angle decreases.

At last, considering the dynamic pressure constraint, if the ballistic coefficient rises, the drag-acceleration drops.

However, just three of these quantities are independent, all the others are subordinate.

The operational altitude is not independent because it is fixed by the aircraft mission, just like the deorbiting altitude. So, these two quantities can't be manipulated too much to move the boundaries.

The ballistic coefficient can be seen as a function of the cross-sectional area and the swept because the mass of the vehicle depends on it using an iterative cycle.

L/D depends on the speed and the angle of attack of the aircraft and its design. In this model, L/D has been evaluated using the minimum value of Mach because it is a stricter condition.

In conclusion, the only performance invariant quantities are the flight path angle, the bank angle, and the cross-section. By manipulating these variables, it's possible to change the shape of the re-entry corridor. The easiest way to do so is to adjust the flight path angle, it has a huge impact on the drag-acceleration, increasing or decreasing the angle by just a few degrees.

4.4 Optimization cycle for re-entry corridor requirements

The procedure followed by Matlab code starts with the definition of range acceptable values for the performance invariant quantities and the drag-acceleration boundaries for total sensed acceleration and dynamic pressure.

At this point, the program requires the inputs that have to be verified by the code. It analyzes them and uses their values to build the re-entry corridor then it checks if the corridor is valid. It checks if the D_{ref3} and D_{ref4} are in the prescribed range, if it's so, the final control is on their mutual placement.

If occurs any problem, the code works in an iterative cycle where the variables are modified to create the corridor setting the right boundaries (as shown in Figure 48). The variables that are easier to manipulate come first.

An example is when D_{ref4} is lower than its minimum value. To make it rise, the first thing is increasing the path angle. If it reaches its maximum value, the swept angle is increased as well. At last, the dimensions of the aircraft can be modified.

On the other hand, if D_{ref4} and D_{ref3} are greater than their respective maximum, the same previous variables can be cut.

After this first cycle, all the other dependent variables are evaluated.

If there is no acceptable result, the program prints it out on the display.

The other cycle is a simultaneous double check on the interaction between D_{ref4} and D_{ref1} and between D_{ref2} and D_{ref1} . If there is no tolerance range between D_{ref4} and D_{ref1} or there is no path between D_{ref2} and D_{ref1} , the easiest thing to do is cut the bank angle. In this way, it can solve the two problems simultaneously.

If the code doesn't converge, the program prints it out on the display.

4.5 Matching Chart

Together with the definition of the re-entry corridor for the second stage, other performance requirements can be set by means of the so-called matching procedure, for both segment of the TSTO. In fact, it is possible to divide an aircraft mission into different phases, each of them has different requirements. The matching chart shows all of them

on a single wing load (WS) vs thrust to lift (TW) graph. Every line on the chart states different requirements and the intersection with the highest T/W is the design point.

Since the model analyzed is the TSTO studied in the previous step, there will be two matching charts, one for each stage, and the input data utilized comes from the optimization cycle results.

Take-off

From statistics, there is an equation that connects WS to TW during take-off (first stage)

$$TW_{to} = \frac{WS}{\sigma Cl_{max} d_{to}}$$

(4.13)

σ is the density correction factor due to airport altitude;

Cl_{max} is the maximum take-off lifting coefficient;

d_{to} is the take-off distance [m].

Climb

The climbing phase is defined from take-off till the aircraft achieves the ceiling altitude (first stage).

During this phase, due to the climbing angle, the thrust balances the drag and partially the aircraft weight, the other portion is balanced by the lift.

The available power generated by the airbreathing engines decreases with the altitude, when it is equal to the power required, the ceiling altitude is

reached. This determines the ambient conditions of temperature and density, establishing the thrust ratio from the nominal condition in their turn.

The WS-TW relation during the climbing phase is

$$TW_{climb} = \frac{A}{WS} + B * WS + C + \sin \alpha$$

(4.14)

A, B, C are three constants defined as

$$A = \frac{0.5 C d_0 \rho_{climb} V_{climb}^2}{W_r}$$

Cd_0 is the zero lift-drag coefficient;

ρ_{climb} is the average air density during the climb [kg/m^3];

V_{climb} is the climbing speed [m/s];

W_r is the weight ratio imposed as 0.95.

$$B = \frac{W_r}{0.5 \rho_{climb} V_{climb}^2 \pi \lambda e}$$

λ is the aspect ratio;

e is the Oswald factor.

$$C = \frac{W_r}{T_r}$$

T_r is the thrust ratio;

α is the climbing angle.

Cruise

During the cruise phase (first stage), the weight is completely balanced by the lift and the drag by the thrust. So the equations that express the relation between WS and TW are the same ruling the climbing angle out, using the average cruise speed, and imposing $W_r=0.7$.

$$TW_{cruise} = \frac{A}{WS} + B * WS + C$$

(4.15)

First stage landing

The first stage of a TSTO comes back to the ground autonomously and lands like a conventional plane. This phase of the aircraft on the matching chart is characterized by a y-axis parallel line whose equation is

$$WS_{1standing} = 0.5 \rho Cl_{maxl} V_l^2 \frac{1}{W_{1r}}$$

(4.16)

Cl_{maxl} is the maximum lifting coefficient;

W_{1r} is the weight ratio between the first stage and the complete vehicle;

V_l is the landing speed [m/s];

ρ is the density at airport altitude [kg/m³].

Orbit Achievement

After the separation from the first stage, the second stage has to reach the target altitude turning the rockets on. On the matching chart, the requirement for orbit achievement is

$$TW = \frac{qCd(1 + \sin \gamma)}{1 - \frac{\Delta V}{Yg_0I_{sp}}}(WS)^{-1}$$

(4.17)

q is the dynamic pressure;

Cd is the drag coefficient;

γ is the climbing angle;

g_0 is the gravitational acceleration;

I_{sp} is the specific impulse;

Y is a parameter defined by the propellant mass and the aircraft weight.

Payload

The equation that defines the payload requirement for the second stage on the matching chart is influenced by different factors, such as second stage geometry, propellant weight on board, operational empty weight, and the payload weight itself. All these components are combined in a single K coefficient and so the equation is

$$TW = \frac{1}{K}WS$$

(4.18)

Re-entry

The second stage, at the end of its mission, has to face the atmosphere re-entry. In order to do so, the vehicle must dissipate all the kinetic energy it has during the descending path. It implies that the aircraft is constantly dragged on its way down to the ground.

On the matching chart, it defines a y-axis parallel line whose equation is

$$WS = \frac{W_{ss}}{2\rho_r C d_r l_d} \left(\frac{V_{de}}{V_{av}} \right)^2$$

(4.19)

W_{ss} is the second stage weight [kg];

ρ_r is the medium re-entry density [kg/m³];

Cd_r is the drag coefficient during re-entry;

l_d is the descending path, evaluated from the deorbit altitude and the descending angle [m];

V_{de} is the deorbit speed [m/s];

V_{av} is the average re-entry speed [m/s].

Second stage landing

At the end of the mission, the second stage of the vehicle has to land like a conventional plane. It is possible to use the same equation defined for the first stage landing.

$$WS_{2standing} = 0.5 \rho C l_{maxl} V_l^2 \frac{1}{W_{2r}}$$

(4.20)

W_{2r} is the weight ratio between the second stage and the complete vehicle.

Boundary 4, Dynamic pressure

Taking a look back at the boundary equations for the re-entry corridor from the previous section, only one of them is influenced by WS. The dynamic pressure constrain is defined by the ballistic coefficient which is highly affected by WS. So reordering the equation it is possible to draw the corresponding line on the matching chart

$$WS = q_{max} Cd D_{ref4}$$

(4.21)

D_{ref4} is the drag deceleration constrain for dynamic pressure.

4.6 Numerical Evaluation

The first step of this work is introducing the geometrical inputs

First Stage			Second Stage		
Minor semi-axis	3.5	m	Minor semi-axis	2	m
Major semi-axis	20	m	Major semi-axis	6	m
Propellant			4000	kg	Payload
					5000 kg

Table 5 Geometrical Inputs

The semi-axis evaluation comes from STRATOFly dimensions, as well for the payload and the propellant.

From these inputs, using a *while* loop, it is possible to calculate the plant surfaces and the weight for both first and second stage.

First Stage			Second Stage		
Surface	857.8	m ²	Surface	215.1	m ²
Weight	448966	kg	Weight	81167	kg

Table 6 Weights and Surfaces

The mission profile defines the operational altitude and the deorbiting altitude

Target Altitude	250 km	Deorbit Altitude	120 km
Orbit Velocity	7756 m/s	Deorbit Velocity	7833 m/s

Table 7 Altitude and Velocity

The attitude of the aircraft in descending path through the atmosphere is defined by two angles chosen according to statistics

γ_e	10.5°	Bank angle	50°
------------	-------	------------	-----

Table 8 Descending Angles

Using these inputs is possible to generate the re-entry corridor thanks to the optimization loop studied in the previous section

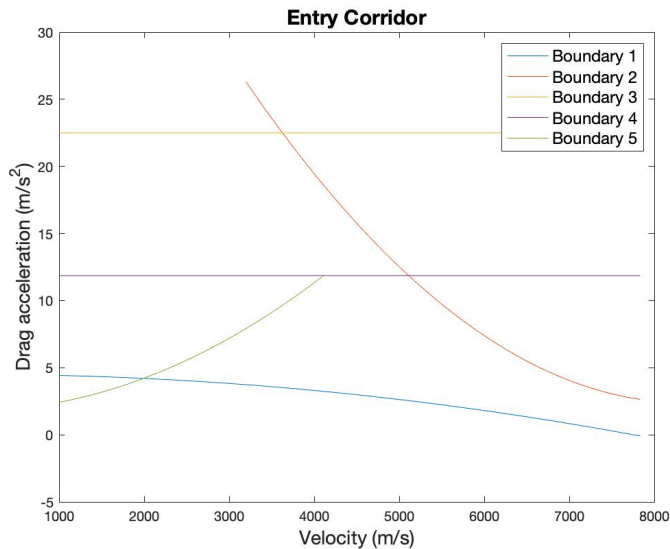


Figure 48 Optimization Cycle Re-entry Corridor

As shown in figure it is possible to note that the total sensed acceleration is less than 3 g's despite the maximum value for that boundary chosen as limit in the cycle is 12 g's, since it is an unmanned vehicle.

Furthermore, the descending path has increased reaching $\gamma_e=10.501^\circ$. Doing so the L/D value has changed as well, flattening the Boundary 1 curve.

The next step is setting the matching chart up. In order to do so, information on take-off and landing for the two stages is requested

First Stage			
Take-off Airport	50 m	Landing Airport	50 m
Take-off Distance	2500 m	Landing distance	4000 m

Second Stage		
Landing Airport	200 m	
Landing distance	4000 m	

Table 9 Take-off and Landing Sites

Take-off and landing distance are evaluated from STRATOFly project. From the same reference

Aspect Ratio	1	CDo	0.016
--------------	---	-----	-------

Table 10 Geometry Inputs

Using the tool displayed in the previous section, it is possible to draw the matching chart for the two stages

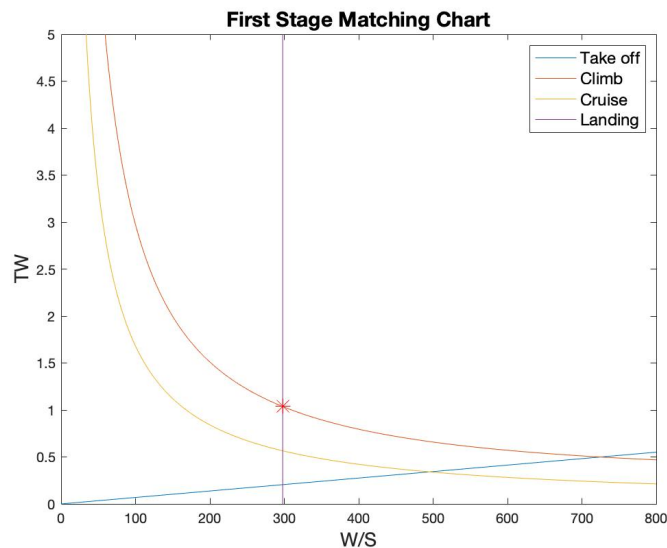


Figure 49 First Stage Matching Chart

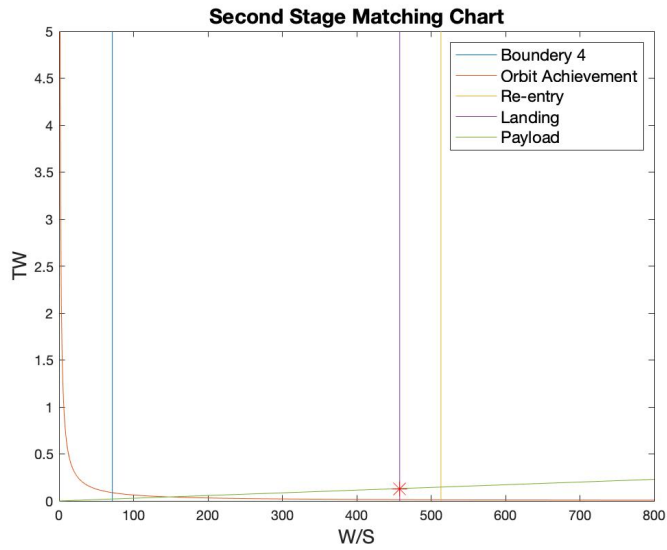


Figure 50 Second Stage Matching Chart

These charts show the design point for first and second stage.

First Stage			
WS	291.06	TS	1.05

Second Stage			
WS	457.84	TS	0.13

Table 11 Design Point

4.7 Comparison with Sanger

The following tables show the main values for the examined TSTO and the Sanger

Sanger Second Stage	
Minor semi-axis	7.8 m
Major semi-axis	13.8 m
Weight	87700 kg

TSTO Second Stage	
Minor semi-axis	2 m
Major semi-axis	6 m
Weight	81168 kg

Sanger First Stage	
Minor semi-axis	20.7 m
Major semi-axis	42.25 m
Weight	259000 kg

TSTO First Stage	
Minor semi-axis	8.5 m
Major semi-axis	20 m
Weight	360220 kg

Table 12 Sanger and TSTO [22]

It is possible to see that the TSTO results are quite similar to the Sanger main data, which means that the optimization cycle is working well.

4.8 Conclusions and future studies

The result of the studies is that if the aircraft has a large flight path angle range, it is possible to build a re-entry corridor whatever the inputs are.

The Matlab code developed for this thesis is a useful high-level tool capable to evaluate a correct aircraft re-entry corridor with a given set of inputs. If these inputs come from the take-off requirements, the program can also provide valid support to reach a full mission requirements optimization.

Playing with the variables, it is possible to notice that the key to the construction of the re-entry corridor is γ_e and the banking angle. By changing these factors almost every configuration is possible.

The code gives also valuable matching charts which deliver realistic design points for the first and the second stage.

The study of this thesis is meant to provide the basis for future studies.

An interesting food for thought is exploring how this new concept could evolve into a new kind of vehicle capable of both taking passengers and payload in space.

Another evolution can be towards a new idea of a cheap launcher that is able to take a second stage to orbit without a rocket.

In any case, a follow-up on the re-entry process is needed if the second stage inputs are modified, like using it as completely reusable access to space.

Space X has stated the path, and now a European response is due.

Bibliography

- [1] CORDIS European Commission,, "Periodic Reporting for period 1 - STRATOFly (Stratospheric Flying Opportunities for High-Speed Propulsion Concepts)," 20 June 2020. [Online]. Available: <https://cordis.europa.eu/project/id/769246/reporting/it>. [Accessed 15 November 2021].
- [2] E. Commission, "Fact sheet: Open Access in Horizon 2020," 9 December 2013. [Online]. Available: https://ec.europa.eu/programmes/horizon2020/sites/default/files/FactSheet_Open_Access.pdf. [Accessed 15 November 2021].
- [3] Polito, "LA NUOVA SFIDA EUROPEA DEL VOLO AD ALTA VELOCITÀ NELLA STRATOSFERA," 2018. [Online]. Available: https://www.researchers.polito.it/success_stories/progetti_horizon2020_coordinati/la_nuova_sfida_europea_del_volo_ad_alta_velocita_nella_stratosfera. [Accessed 15 November 2021].
- [4] E. C. I. a. N. E. Agency, "STRATOFly," [Online]. Available: <https://ec.europa.eu/inea/en/horizon-2020/projects/h2020-transport/aviation/stratofly>. [Accessed 15 November 2021].
- [5] CORDIS European Commission, "Stratospheric Flying Opportunities for High-Speed Propulsion Concepts," 9 June 2020. [Online]. Available: <https://cordis.europa.eu/project/id/769246/reporting/it>. [Accessed 15 November 2021].
- [6] S. E. J. T. Langener*, "TRAJECTORY SIMULATION AND OPTIMIZATION OF THE LAPCAT-MR2 HYPERSONIC CRUISER CONCEPT," in *29th International Congress of the International Council of Aeronautical Science*, 2014.
- [7] J. Steelant and O. Haidn, "Achievements Obtained for Sustained Hypersonic Flight Within the LAPCAT Project," in *15th AIAA International Space Planes and Hypersonic Systems and Technologies Conference*, 2008.

- [8] J. Steelant, "Achievements Obtained for Sustained Hypersonic Flight within the LAPCAT project.," in *15th AIAA International Space Planes and Hypersonic Systems and Technologies Conference*, Dayton, Ohio, 2018.
- [9] V. Fernández-Villacè, G. Paniagua and J. Steelant, "Installed performance evaluation of an air turbo-rocket expander engine," *Aerospace Science and Technology*, vol. 35, pp. 63-79, 2014.
- [10] C. Meerts and J. Steelant, "Air Intake Design for the Acceleration Propulsion Unit of the LAPCAT-MR2 Hypersonic Aircraft," in *5TH EUROPEAN CONFERENCE FOR AERONAUTICS AND SPACE SCIENCES (EUCASS)*.
- [11] L. Nista and B. H. Saracoglu, "Numerical investigation of the STRATOFLY MR3 propulsive nozzle during supersonic to hypersonic transition," in *AIAA Propulsion and Energy 2019 Forum*, 2019.
- [12] V. Fernandez Villace and J. Steelant, "The Thermal Paradox of Hypersonic Cruisers," in *International Space Planes and Hypersonic Systems and Technologies Conferences*, Glasgow, 2015.
- [13] R. Fusaro, D. Ferretto, v. Vercella, N. Viola, V. Fernandez Villace and J. Steelant, "A methodology for preliminary sizing of a Thermal and Energy Management System for a hypersonic vehicle.," in *ICAS*, 2018.
- [14] C. Weiland and C. Weiland, *Aerodynamic Data of Space Vehicles*, Springer, 2014.
- [15] D. R. Jenkins, T. Landis and J. Miller, *AMERICAN X-VEHICLES*, 2003.
- [16] E. Heinrich and C. Weiland, *Selected Aerothermodynamic Design Problems of Hypersonic Flight Vehicles*, Springer, 2009.
- [17] A. Marèe, E. Mooij and B. Zandbergen, *Space-Plane Analysis*.
- [18] P. Lu, "Asymptotic Analysis of Quasi-Equilibrium Glide in LiftingEntry Flight," *Journal of Guidance, Control, and Dynamics*, vol. 29, no. 3, p. 662–670, 2006.

- [19] W. J. Larson and L. K. Pranke, Human Space Flight: Mission Analysis and Design.
- [20] J. D. Anderson, Hypersonic and High-Temperature Gas Dynamics, American Institute of Aeronautics and Astronautics, Inc..
- [21] D. H. Kerry, Introduction to Astrodynamic Re-entry.
- [22] Koelle, "SÄENGER II, A Hypersonic Flight and Space TransportationSystem".